Doctoral Dissertation

博士論文

Behavioral analysis of schizophrenia-like phenotypes in a mouse model of 22q11.2 deletion syndrome

(22q11.2 欠失症候群モデルマウスの作製と行動学的手法による統合失調症様表現型の解析)

A Dissertation Submitted for Degree of Doctor of Philosophy

December 2019

令和元年 12 月 博士 (理学) 申請

Department of Biological Sciences,
Graduate School of Science, The University of Tokyo

東京大学大学院理学系研究科生物科学専攻

Ryo Saito

齋藤　遼

Abstract

The 22q11.2 deletion syndrome (22q11.2DS) is associated with an increased risk for psychiatric disorders. Although most of the 22q11.2DS patients have a 3.0-Mb deletion, current mouse models only mimic a minor mutation of 22q11.2DS, a 1.5-Mb deletion. The role of the genes existing outside the 1.5-Mb deletion in psychiatric symptoms of 22q11.2DS is unclear. In this study, I generated a mouse model that reproduced the 3.0-Mb deletion of the 22q11.2DS (*Del(3.0Mb)/+*) using the CRISPR/Cas9 system. Ethological and physiological phenotypes of adult male mutants were comprehensively evaluated by visual evoked potentials, circadian behavioral rhythm and series of behavioral tests such as measurement of locomotor activity, sociability, prepulse inhibition, fear-conditioning memory and visual discrimination learning. As a result, *Del(3.0Mb)/+* mice showed reduction of auditory prepulse inhibition and attenuated cue-dependent fear memory, which is consistent with the phenotypes of previous 22q11.2DS models. Additionally, *Del(3.0Mb)/+* mice displayed an impaired early visual processing that is commonly seen in patients with schizophrenia. Meanwhile, unlike the previous models, *Del(3.0Mb)/+* mice exhibited hypoactivity over several behavioral tests, possibly reflecting the negative symptoms of schizophrenia or the fatigability of 22q11.2DS patients. Lastly, *Del(3.0Mb)/+* mice displayed a faster adaptation to experimental jet lag as compared to wild-type mice. These results support the validity of *Del(3.0Mb)/+* mice as a schizophrenia animal model and suggest that this mouse model is a useful resource to understand pathogenic mechanisms of schizophrenia and other psychiatric disorders associated with 22q11.2DS.

~ Contents ~

Abbreviations

22q11.2DS	22q11.2 deletion syndrome
ACFS	artificial cerebrospinal fluid
ADHD	attention deficit hyperactivity disorder
ANOVA	analysis of variance
ARSA	aberrant right subclavian artery
ATP	adenosine 5'-triphosphate
CaMKII	calcium/calmodulin-dependent protein kinase II
Cas9	CRISPR-associated 9
cDNA	complementary DNA
CGH	comparative genomic hybridization
CNV	copy number variation
CRISPR	clustered regularly interspaced short palindromic repeats
cRNA	complementary RNA
CT	circadian time
Cy3	cyanine 3
D-AP5	D-(-)-2-amino-5-phosphonopentanoic acid
dB	decibel
DD	constant darkness
DNA	deoxyribonucleic acid
DSB	double-strand break
dT	deoxythymidine
EDTA	ethylenediaminetetraacetic acid
EGTA	ethylene glycol tetraacetic acid

ES	embryonic stem
FDR	false discovery rate
Fw	forward
GWAS	genome wide association study
HEPES	4-(2-hydroxyethyl)-1-piperazineethanesulfonic acid
IAA	interrupted aortic arch
LCRs	low copy repeats
LD	light-dark
LED	light emitting diode
LFP	local field potential
mEPSC	miniature excitatory postsynaptic current
mIPSC	miniature inhibitory postsynaptic current
miRNA	microRNA
mPFC	medial prefrontal cortex
mRNA	messenger RNA
mWM	modified Whitten's medium
NAHR	non-allelic homologous recombination
NBQX	2,3-Dioxo-6-nitro-1,2,3,4-tetrahydrobenzo[f]quinoxaline-7-sulfonamide
NCBI	National Center for Biotechnology Information
nt	nucleotide
PAM	protospacer adjacent motif
PB	phosphate buffer
PCR	polymerase chain reaction
PFA	paraformaldehyde

PMT	photomultiplier tube
PPI	prepulse inhibition
RMA	robust multi array average
RNA	ribonucleic acid
RT	reverse transcription
Rv	reverse
SCN	suprachiasmatic nucleus
SD	standard deviation
SEM	standard error of mean
sgRNA	single-guide RNA
SNP	single nucleotide polymorphism
ssODN	single-stranded oligodeoxyribonucleotide
TE	Tris-EDTA buffer
TTX	tetrodotoxin
VD	visual discrimination
VEP	visual evoked potential
WT	wild-type
XDR	external data representation
ZT	zeitgeber time

Chapter 1. Introduction

1.1 Schizophrenia

Schizophrenia is a serious mental disorder that affects approximately 1% of the total population of the world. The onset of schizophrenia typically begins during adolescence or early adulthood. This disorder interferes with a person's thinking, emotion and behavior, which results in impaired activity of daily life and social relationship. The symptoms of schizophrenia are characterized by three categories: positive symptoms, negative symptoms and cognitive dysfunctions. Positive symptoms include delusions and hallucinations. Negative symptoms include flatting of affect, loss of a sense of pleasure, loss of motivation and social withdrawal. In the cognitive dysfunctions, various obstacles including deficits in attention, working memory, verbal learning and executive functions are observed. Because the onset mechanisms of these symptoms are unclear, elucidating biological mechanisms underlying schizophrenia is an important challenge.

1.2 Genetic risk factor of schizophrenia

Genetic epidemiological research such as twin and family-based study focused on schizophrenia has suggested that genetic factors are involved in an increased risk of schizophrenia. For instance, familial aggregation of schizophrenia has been recognized in family-based studies, and the prevalence of schizophrenia in individuals with an affected first-degree relative is higher than in the general population (Chou et al., 2017). In addition, twin studies have shown that the concordance rate for schizophrenia was elevated in monozygotic twins (approximately 50%) compared to dizygotic twins (approximately 15%) (Cardno and Gottesman, 2000), indicating that there is a genetic contribution for the enhanced risk of schizophrenia.

Moreover, many single nucleotide polymorphisms (SNPs) that are suspected of contributing to the onset of schizophrenia were identified by genome-wide association study (GWAS).

However, the impact of a SNP on the development of schizophrenia is small (odds ratio: 1.09–1.25) (O'Donovan et al., 2008; Purcell et al., 2009; Rietschel et al., 2012; Ripke et al., 2011; Shi et al., 2011; Steinberg et al., 2011; Williams et al., 2011). On the other hand, some chromosome structure variations, which are referred to as copy number variations (CNVs), have been found in the patient population of schizophrenia by GWAS (e.g. 1q21.1 deletion, 7q36.3 duplication, 16p11.2 duplication, 17q12 deletion and 22q11.2 deletion) (Levinson et al., 2011; Moreno-De-Luca et al., 2010; Vacic et al., 2011). A CNV is defined as a copy number alteration in a DNA segment that is over 1 kb in length on the chromosome in comparison with a reference genome (Feuk et al., 2006). Chromosomal structural variations include deletions, duplications and insertions. Although these CNVs are infrequent in the overall population (less than 1% frequency), the effect on the onset of schizophrenia is about 10-fold higher than that of a SNP. Among them, 22q11.2 deletion has the highest risk of schizophrenia, indicating one of the important genetic risk factors of schizophrenia.

1.3 22q11.2 deletion syndrome

The 22q11.2 deletion syndrome (22q11.2DS) is the most common chromosomal microdeletion disorder in humans, with an estimated incidence of 1 in 1,000 to 4,000 live births (Devriendt et al., 1998; Grati et al., 2015; Wapner et al., 2012). Individuals with this syndrome display multiple physical abnormalities; cardiac malformation is the most frequent symptom affecting approximately 80% of patients, followed by less frequent symptoms such as velopharyngeal insufficiency, hypocalcemia, thymus hypoplasia and immune deficiency (Botto et al., 2003; Ryan et al., 1997). Additionally, 22q11.2DS is known to increase the risk of developing a variety of psychiatric and developmental disorders including schizophrenia, intellectual disability, autism spectrum disorder, attention deficit hyperactivity disorder (ADHD), early-onset Parkinson's

disease and sleep behavior disorder (Bassett et al., 2005; Buckley et al., 2017; Gothelf et al., 2004; Mok et al., 2016; Niklasson et al., 2009). The total penetrance for psychiatric disorders reaches 100% in 22q11.2DS (Kirov et al., 2014). As mentioned above, particularly, the risk of schizophrenia imposed by this deletion (odds ratio; 16.3–44.2) is higher than any other schizophrenia-associated single genetic variations that have been reported so far (Grozeva et al., 2012; Stone et al., 2008; Szatkiewicz et al., 2014). Therefore, studying 22q11.2DS will shed light on the pathogenesis of schizophrenia.

Most (~90%) of individuals affected with 22q11.2DS have a 3.0-Mb hemizygous deletion on chromosome 22q11.2 (Carlson et al., 1997; Emanuel, 2008; Guo et al., 2018; Kushima et al., 2018; Michaelovsky et al., 2012). Less frequently, approximately 7% of the patients have a half of the 3.0-Mb deletion (referred to as 1.5-Mb deletion), and fewer patients have the other half of the 3.0-Mb deletions (referred to as 1.4-Mb deletion) (Carlson et al., 1997; Emanuel, 2008; Lopez-Rivera et al., 2017). These chromosomal deletions result from a meiotic unequal non-allelic homologous recombination (NAHR) event induced by multiple segmental duplications (low copy repeats: LCRs), termed LCR22s (Figure 1). The several large size LCR22s (referred to as LCR22A, B, C and D) are located in the 3.0-Mb region on chromosome 22q11.2. The most frequent 3.0-Mb deletion is caused by NAHR events between LCR22A and LCR22D, and the 1.5-Mb deletion and 1.4-Mb deletion were induced by unequal crossing over between LCR22A and B and between LCR22B and D, respectively (Burnside, 2015; Edelmann et al., 1999; Shaikh et al., 2001).

1.4 22q11.2DS mouse models

Forty-five protein coding genes are located within the 3.0-Mb deleted region and 37 of them are conserved in the mouse chromosome 16qA13 (Guna et al., 2015; Puech et al., 1997), making it

possible to generate a mouse model of 22q11.2DS. To date, four lines of 22q11.2DS mouse models have been generated and analyzed (Figure 2; Lindsay et al., 1999; Merscher et al., 2001; Nilsson et al., 2016; Stark et al., 2008). However, all of them mimicked the 1.5-Mb deletion (LCR22A–B deletion), and the contributions to this syndrome of the genes on the locus between LCR22B and D were poorly understood. Previously, Michaelovsky and colleagues have reported that a patient with the LCR22B–D deletion is suffering from severe anxiety disorders and the predominantly inattentive type of ADHD (Michaelovsky et al., 2012). Therefore, there is possibility that key genes located in the 1.4-Mb deleted region are responsible for the development of psychiatric disorders. Furthermore, although the behavioral analyses of these 22q11.2DS mouse models were repeatedly conducted, the results were still controversial, depending on the behavioral paradigms (Table 1). It is known that a difference of the genetic background gives rise to variable phenotypic expression (Hiroi, 2018; Sittig et al., 2016). These 22q11.2DS mouse models, except for *Df(h22q11)/+*, were generated by introducing the deletion into the donor chromosome from different strain. Thus, it is difficult to compare their phenotypes correctly, although most of them were backcrossed with C57BL/6 strain. With the advent of genome editing technologies applied directly in mouse zygotes (Boroviak et al., 2016; Cong et al., 2013; Kraft et al., 2015; Wang et al., 2014), it is possible to obtain mutant mice in a pure C57BL/6N background, the most popular strain of laboratory mouse.

1.5 Large-scale chromosomal engineering by CRISPR/Cas9 systems

As above, chromosomal rearrangements or structure variations of genomic regions is the cause of some human genetic diseases such as DiGeorge syndrome (22q11.2DS), Williams syndrome (7p11.23 deletion) and Smith-Magenis syndrome (17q11.2 deletion). Because genes contained in these deletion regions tend to be conserved between humans and mice, the modeling

chromosomal variations involved in human genetic variations with mice is feasible and effective experimental approach. Typically, chromosomal modifications in mouse genome have been conducted using Cre-*loxP* recombination (Herault et al., 1998; Ruf et al., 2011; Spitz et al., 2005). The desired genomic structure alterations can be introduced into embryonic stem (ES) cells by the Cre-recombination of targeted *loxP* sequences in mouse chromosome (Ramirezsolis et al., 1995; Smith et al., 1995). Subsequently, mutant chimeric mice are generated via injection of mutant ES cell clones into the blastocoel cavity of blastocysts (Bradley et al., 1984), and then desired F1 mice are established by crossing the chimeric mouse with a wild-type (WT) mouse. So far, many mouse models of human genetic diseases have been generated using Cre-*loxP* recombination (Li et al., 2009; Lindsay et al., 1999; Merscher et al., 2001; Nilsson et al., 2016; Stark et al., 2008; Walz et al., 2003). However, because the multi-step procedure is required for generation of mutant mice by Cre-*loxP* system, this method is time consuming and laborious. Additionally, in many cases, because the different origin of ES cells and blastocysts are used, the obtained mutant is a hybrid and their genetic background is not unified.

In recent years, clustered regularly interspaced short palindromic repeat (CRISPR)/CRISPR-associated protein 9 (Cas9) systems have been developed as an available genome editing technology (Cong et al., 2013; Mali et al., 2013; Wang et al., 2013). Originally, CRISPR/Cas9 systems are discovered as an adaptive immune mechanism of bacteria and archaea to protect themselves against invading genetic elements, such as plasmids and bacteriophages (Barrangou, 2013; Barrangou et al., 2007; Gasiunas et al., 2012; Ishino et al., 1987; Jansen et al., 2002). The RNA-guided Cas9 nuclease can introduce a double-strand break (DSB) at a specific site based on a guide RNA (gRNA)-defined target sequence in order to excluding foreign genetic elements (Figure 3). Application of this mechanism enables us to introduce mutations in any location on the genomic sequence of model organisms. The CRISPR/Cas9 is preferred as a

standard method that can save time and effort as compared with conventional genome editing in ES cells. In addition, because this approach can be applied directly in mouse zygotes, it is able to generate mutant mice that maintain pure genetic background. Furthermore, the CRISPR/Cas9 technology have been successfully utilized for introducing structural variations at the large scale (megabase level) with high efficiency in mice (Boroviak et al., 2016; Kraft et al., 2015). In the present study, I attempted to generate a 22q11.2DS mouse model with a unified genetic background by chromosomal rearrangement using the CRISPR/Cas9 system in mouse zygotes.

1.6 Aim of this study

To decipher the pathogenic mechanisms of schizophrenia as well as 22q11.2DS, I tried generation of a novel mouse model with higher validity as schizophrenia model than previous 22q11.2DS models and investigation of its phenotypes with multifaced analyses related to psychiatric disorders. Furthermore, to find a new phenotype associated with psychiatric disorders, I evaluated the visual evoked potentials and circadian behavioral rhythm.

Chapter 2. Materials and methods

2.1 Animals

Animals were housed under a 12 h light/dark cycle (light on at 08:00, off at 20:00), with free access to food and water, at temperature maintained at 23 ± 1°C. The animal experiments were approved by the Institutional Animal Care and Use Committee of The University of Tokyo and the ethics committee of Nagoya University, and conducted in accordance with the guidelines of The University of Tokyo and Nagoya University.

2.2 Preparation of *Cas9* mRNA, single-guide RNAs (sgRNAs) and a single-stranded oligodeoxyribonucleotide (ssODN)

I used CRISPRdirect software to design sgRNA with smaller number of off-target sites, [http://crispr.dbcls.jp (Naito et al., 2015)]. Two pairs of sgRNAs were positioned on either endpoint of the deletion. The protospacer sequences of sgRNAs were listed in Table 2. I constructed pDR274 plasmids (Addgene #42250) carrying each of the sgRNA. The sgRNAs were transcribed *in vitro* using the *Dra*I-digested pDR274 vectors as a template and the MEGAshortscript T7 kit (Ambion, CA, USA) according to manufacturer's instruction. The synthesized sgRNAs were then purified using MEGAclear kit (Ambion) according to manufacturer's instruction. The *Cas9* mRNA was transcribed *in vitro* using an *Age*I-digested Cas9 expression vector, pcDNA3.1-hCas9 (Nakao et al., 2016), as templates and the MessageMax T7 ARCA-Capped Message mRNA transcription kit (Cellscript, WI, USA) according to the manufacturer's instruction. The poly(A) tailing reaction was performed using A-plus Poly(A) Polymerase Tailing kit (Cellscript) according to the manufacturer's instruction. *Cas9* mRNA was then purified using MEGAclear kit (Ambion) according to the manufacturer's instruction. The ssODN designed to bridge the deletion endpoints was 120 nucleotides in length

and positioned directly adjacent to the most external sgRNA site. The ssODN was synthesized by Integrated DNA Technologies, Inc. (Iowa, USA).

2.3 Microinjection of *hCas9* mRNA, sgRNAs and ssODN

Fifty ng/μL of *hCas9* mRNA, 25 ng/μL of sgRNA (each) and 100 ng/μL of ssODN were mixed in RNase-free water and microinjected into the cytoplasm of C57BL/6N (Charles River Laboratories Japan Inc., Kanagawa, Japan) fertilized eggs. Survived microinjected embryos were cultured in modified Whitten's medium (mWM) until the 2-cell stage. Injected embryos were transferred into oviducts of 0.5-day-post-coitum recipients (ICR, Charles River Laboratories Japan Inc.). Obtained founder candidate mice were genotyped and crossed with C57BL/6N mice to obtain N1 mice.

2.4 Genotyping of 22q11.2DS mice by PCR assay

The screening of mutant mice was performed by PCR assay using Ex *Taq* DNA polymerase (Takara Bio Inc., Shiga, Japan). Genomic DNA was extracted from placenta or tail tips of mice or embryos. The following primers were used for genotyping: Del3.0Mb-Fw, 5'-CTTGCATATTTCACGGAGGCG-3'; Del3.0Mb-Rv, 5'-CAAGTAGAGAGGGAGTGGTGC-3'. The PCR condition was 98°C for 2 min, 30 cycles of melting at 98°C for 30 s, annealing at 65°C for 30 s, and extension at 72°C for 30 s, with additional extension at 72°C for 2 min at the end. PCR products were analyzed in 1% agarose gel electrophoresis and the sequences were confirmed by Sanger sequencing (Fasmac Co., Kanagawa, Japan).

2.5 Array comparative genomic hybridization (CGH) analysis

Array CGH was performed using an Agilent SurePrint G3 Mouse CGH 4x180K Microarray

(Agilent, Santa Clara, CA, USA) according to the manufacturer's instructions. CNV calls were made with Nexus Copy Number software v9.0 (BioDiscovery, El Segundo, CA, USA) using the Fast Adaptive States Segmentation Technique 2 (FASST2) algorithm, which is a hidden Markov model-based approach. The $\log_2$ ratio threshold for copy number loss (or deletion) was set at −0.4. The significance threshold to adjust the sensitivity of the segmentation algorithm was set at 1×10^{-6}, and at least five contiguous probes were required for CNV calls. Genomic locations are reported in NCBI Build 37/UCSC mm9 coordinates.

2.6 RNA extraction

Total RNA was isolated from hippocampi or frontal cortexes of *Del(3.0Mb)/+* male (n = 5) and WT littermate male (n = 5) using miRNeasy Mini Kit (QIAGEN, MD, USA).

2.7 mRNA microarray analysis

Preparation of cRNA, hybridization, and scanning of microarrays were performed according to the manufacturer's protocol. Briefly, biotinylated cRNAs were synthesized by GeneChip 3' IVT PLUS Reagent Kit (Affymetrix, CA, USA) from 250 ng total RNA. Biotinylated cRNA yields were checked with the NanoDrop ND-2000 Spectrophotometer. Following fragmentation, 15 μg of cRNA was hybridized for 16 h at 45°C on GeneChip Mouse Genome 430 2.0 Array. Arrays were then washed and stained in the GeneChip Fluidics Station 450 (Affymetrix), followed by scanning in an Affymetrix 3000 7G scanner. Background subtraction, normalization and summarization were performed using the robust multi array average algorithm (RMA) method by Expression Console Software (Affymetrix). I analyzed 3 *Del(3.0Mb)/+* mice and 3 WT mice. An empirical Bayes moderated *t*-statistics was calculated by using limma eBayes package. Benjamini and Hochberg's FDR was used to control false positives caused by multiple testing.

2.8 miRNA microarray analysis

Preparation of labeled miRNA, hybridization, and scanning of microarrays were performed according to the manufacturer's protocol. Cyanine 3 (Cy3) labeled miRNA was prepared from 100 ng total RNA using the miRNA Complete Labeling and Hyb Kit (Agilent). The dried Cy3-labeled miRNA was resuspended in 18 μL of nuclease-free water, then 4.5 μL of the 10xGE Blocking Agent and 22.5 μL of 2× HiRPM Hybridization Buffer were added. After incubation at 100°C for 5 min, the samples were immediately transferred to an ice water bath and hybridized to Mouse miRNA V21.0 Microarray (Agilent) at 55°C for 20 h in a rotating Agilent hybridization oven. After hybridization, microarrays were washed with GE Wash Buffer 1 (Agilent) at room temperature for 5 min and with GE Wash Buffer 2 (Agilent) at 37°C for 5 min, then dried immediately. Microarrays were scanned immediately after washing on the Agilent SureScan Microarray Scanner (G2600D) using one color scan setting for 8x15k array slides (Scan Area 61 × 21.6 mm, Scan resolution 5 μm, Dye channel is set to Green PMT is set to XDR Hi 100% and XDR Lo 5%). The scanned images were analyzed with Feature Extraction Software 12.0.3.1 (Agilent) using default parameters to obtain background subtracted and spatially detrended Processed Signal intensities. The GeneView files were generated using Agilent Feature Extraction software version 12.0.3.1. I analyzed 3 *Del(3.0Mb)*/+ mice and 3 WT mice. For statistical analysis, we used a set of miRNAs that were detected in all the 6 samples (428/1881 (22.8%) in the hippocampus; 484/1881 (25.7%) in the frontal cortex).

2.9 Quantitative RT-PCR

For quantification of mRNA, first strand cDNA was synthesized using PrimeScript RT reagent Kit (Perfect Real Time) (Takara Bio) according to the manufacturer's instruction. Briefly, 300 ng of total RNA was reverse transcribed using 25 pmol of oligo dT primer and 50 pmol of random

6 mer in 10 μL reaction. The resultant cDNA was diluted at 1:30 ratio in TE buffer (pH 8.0). For quantification of miRNA, cDNA was synthesized using Mir-X miRNA First-Strand Synthesis Kit (Takara Bio) according to the manufacturer's instruction. Briefly, ~1 μg of total RNA was reverse transcribed in 10 μL reaction. The resultant cDNA was diluted at 1:10 ratio in nuclease-free water. All samples within an experiment were reverse transcribed at the same time. All real-time PCR reactions were performed using the PowerUp SYBR Green Master Mix (Applied Biosystems, CA, USA) and the StepOnePlus Real-Time PCR system (Applied Biosystems). The experiments were carried out in triplicate for each data point. The relative quantification in gene expression was determined using ΔΔCt method (Livak and Schmittgen, 2001). The sequences of the primers are listed in Table 3.

2.10 Histology

In order to obtain the embryos, I conducted *in vitro* fertilization between C57BL/6N WT eggs and N1 *Del(3.0Mb)/+* sperm. Subsequently, viable 2-cell embryos were transferred into oviducts of pseudopregnant ICR mice. Embryos (N2) were isolated from 18.5-day pregnant female mice by the Cesarean section, where the day of vaginal plug was scored as embryonic day (E) 0.5. Samples were subjected to a thoracic incision and fixed with 4% paraformaldehyde (PFA) in 0.1 M phosphate buffer (PB; pH 7.4), at 4°C overnight. Then, organs were dissected and observed using stereoscopic microscope LEICA MZ6 (Leica, Wetzlar, Germany) and camera IC90E (Leica).

2.11 Behavioral tests

Del(3.0Mb)/+ mice and WT control littermates were obtained by *in vitro* fertilization between C57BL/6N eggs and *Del(3.0Mb)/+* sperm. One cohort of mice (WT, n = 13; *Del(3.0Mb)/+*, n =

9) was used for open field test, visual prepulse inhibition (visual PPI), five-trial direct social interaction test and contextual and cued fear-conditioning test. A second cohort of mice (WT, n = 15; *Del(3.0Mb)*/+, n = 15) was used for Y-maze test, elevated-plus maze test, locomotor activity, three-chamber sociability and social preference test, auditory PPI and rotarod test. A third cohort of mice (WT, n = 7; *Del(3.0Mb)*/+, n = 6) was used for visual discrimination task and reversal learning. All behavioral tests were carried out with male mice at the age of 2–5 months. Prior to behavioral tests, mice were placed in the testing room for at least 1 h to acclimate to the experimental environments. The experimenter was blind to genotype throughout the experimental procedures. Detailed information of the behavioral methods is described below.

2.11.1 Open field test

Mice were placed in the center of the open field (diameter: 75 cm, height: 35 cm) and were allowed to explore freely the arena for the following 10 min under moderately light conditions (15 lux). Their movement was recorded with a camera mounted above the arena, and their activity was measured automatically using smart 3.0 software (Bio Research Center Co. Ltd., Nagoya, Japan). The open field was divided into an inner circle (diameter: 50 cm), and an outer area surrounding the inner circle. Measurements included total distance moved and time spent in the inner and outer sections. The open field arena was cleaned with 70% ethanol and wiped with paper towels between each trial.

2.11.2 Locomotor activity under the novel environment

Each individual mouse was placed in a standard transparent rectangular rodent cage (25 cm × 30 cm × 18 cm) under moderately light conditions (15 lux). The movement of mice was detected for 120 min using a pyroelectric infrared sensor (NS-AS01; Neuroscience Inc, Tokyo, Japan) placed

over the cage and locomotor activity was measured using Digital acquisition system (NS-DAS-8; Neuroscience Inc.).

2.11.3 Rota-rod test

I performed the rotarod test using Rota-rod treadmill for mice MK-600 (Muromachi Kikai Co., Ltd., Japan). The apparatus consists of a set of five horizontal rods. These rods are separated by opaque disks. Hence, test mice cannot be distracted from one another. Mouse was placed on a still rod for 1 min. Then, the rotation was started and the time length before fall was recorded. The speed of the rod's rotation was 6 rpm in the training session of 3 consecutive days (day1–3) and 12 rpm in the test session (day4). Six trials per day were carried out, and a maximum time length for each training was 2 min. The inter-trial interval was 15 min.

2.11.4 Elevated plus-maze test

The elevated plus-maze consists of two opposing open (25 cm × 8 cm) and two close arms (25 cm × 8 cm × 20 cm), linked by a neutral area (8 cm × 8 cm) in the center of the apparatus. The entire apparatus was elevated to height of 50 cm above floor level. The light intensity around the maze was set at 100 lux. Mice were placed in the central platform facing an open arm and allowed to move freely through the maze for 5 min. Their behavior was recorded with a camera mounted above the apparatus. Measurements included the number of entries to and close arms entries and time spent open and close arms. The maze was cleaned with 70% ethanol and wiped with paper towels between each trial.

2.11.5 Three-chamber sociability and social novelty tests

The sociability and social novelty tests apparatus is a rectangular, three-chambered opaque

Plexiglas boxes (each box is 20 cm long, 40.5 cm wide, 22 cm high). Dividing walls were made from clear Plexiglas, with small square openings allowing access into each chamber. A small cylindrical cage made of Plexiglas with multiple holes (diameter: 7 cm, height: 12 cm) was used as the cage enclosing a stranger mouse, which allowed nose contact through the holes, but prevented fighting. A weight (cup) was placed on the top of the cage to prevent the test mouse from climbing. Two cylindrical cages were located in the left and right chambers during the trial. The chambers of the social apparatus and two cylindrical cages were cleaned with 70% ethanol and wiped with paper towels between each trial. Before testing day, mice were individually habituated to the apparatus, with 10 min of free exploration period for 3 consecutive days. On the testing day, the test mouse was placed in the middle chamber and allowed to explore freely for 10 min (habituation phase). After habituation phase, an unfamiliar C57BL/6J mouse with the same age and sex (stranger1) that had no prior contact with the subject mice, was placed in one of the side boxes. The cylindrical cage on the other side remained empty. The location of stranger 1, the left versus right side chamber was systematically alternated between trials. The test mouse was placed in the middle chamber and allowed to explore freely the entire test box for 10 min. Sniffing zone was defined as the range of 10 cm in radius from each center point of cylindrical cages. Time spent in each box and in each sniffing zone, and the number of entries into each box were recorded using Ethovision automated tracking program (Brainscience Idea Co., Ltd., Osaka, Japan) to measure the sociability. After the end of the first 10 min, each mouse was subjected to the a second 10-min session to measure social preference for a new stranger. In the second session, unfamiliar mouse was placed in the box that had been empty during the first 10-min session. This second stranger (stranger 2) was also enclosed in an identical small cylindrical cage. The test mouse had a choice between the stranger 1 and stranger 2. As described above, time spent in each box and in each sniffing zone, and the numbers of entries into each box were recorded to measure the

preference for social novelty.

2.11.6 Five-trial direct social interaction test

Subject mice were placed individually into home cage (45 cm × 28 cm × 16 cm) for 1 h before starting test under the moderately light conditions (15 lux). A juvenile intruder mouse (5-week-old) was introduced into the subject mouse's home cage. The subject mouse was exposed to the same intruder mouse for 5 min over 4 trials with an inter-trial-interval of 30 min. During the fifth trial, the subject was exposed to a novel intruder mouse (5-week-old). The time spent in social interaction (close following, inspection, anogenital sniffing, and other social body contacts) was recorded.

2.11.7 Auditory prepulse inhibition

The auditory prepulse inhibition (PPI) test was performed by using SR-Lab system (San Diego Instruments, San Diego, CA, USA). A standard startle chamber applicable to mice and rats (San Diego Instruments) was used. The startle chamber consisted of a Plexiglas cylinder for mice (105 mm, 38 mm inner diameter, 50 mm outer diameter) and was placed in a sound-attenuated chamber, in which the animals were individually placed. The cylinder was mounted on a plastic frame under which a piezoelectric accelerometer was placed to record and transduce the vibrations of the cylinder. After the animals were placed in the chamber under moderately bright light conditions (180 lux), they were allowed to acclimate for 10 min, during which they are exposed to 65 dB background white noise was continually present. Individual mouse then received 10 startle trials, 10 no-stimulus trials and 40 PPI trials. The inter-trial interval was between 10 and 20 s and each session lasted 17 min. The startle trial consisted of a single 120 dB white noise burst lasting 40 ms. PPI trials consisted of a prepulse (20 ms burst of white noise at

69, 73, 77 or 81-dB intensity) followed by the startle stimulus (120 dB, 40 ms white noise) 100 ms later. Each of the four prepulse trials (69, 73, 77 or 81 dB) was done 10 times. Sixty different trials were performed pseudorandomly to ensure that each trial was done 10 times and that no two consecutive trials were identical. The movement of the animal in the startle chamber was measured for 100 ms after the onset of startle stimulus onset (sampling frequency 1 kHz), rectified, amplified and processed by a computer, which calculated the maximal response over the 100-ms period. Basal startle amplitude was determined as the mean amplitude of the 10 startle trials. PPI (%) was calculated as follows: 100 × (pulse-alone response − prepulse-pulse response)/pulse-alone response, in which prepulse-pulse response was the mean of the 10 PPI trials (69, 73, 77 or 81 dB) and pulse-alone response was the basal startle amplitude.

2.11.8 Visual prepulse inhibition

The visual prepulse inhibition (PPI) test was conducted as previously described (Aubert et al., 2006) with minor modifications. The visual prepulse was created by turning on nine light-emitting diode (LED) light bulbs in startle chamber. The light instrument was located 8 cm above the Plexiglas cylinder and the light condition of the chamber was dim (2 lux). In this test, two conditions of light prepulse duration (20 or 25 ms) were tested. The light intensity was fixed at 900 lux. After the animals were placed in the chamber, they were allowed to acclimate for 10 min, during which they are exposed to 65 dB background white noise was continually present. Individual mouse then received 10 startle trials, 10 no-stimulus trials and 20 PPI trials. The inter-trial interval was between 10 and 20 s. The startle trial consisted of a single 120 dB white noise burst lasting 40 ms. PPI trials consisted of a light prepulse (900 lux, 20 or 25 ms duration) followed by the startle stimulus (120 dB, 40 ms white noise) 100 ms later. Each of the two prepulse trials (20 or 25 ms) was done 10 times. Forty different trials were presented

pseudorandomly, to ensure that each trial was done 10 times and that no two consecutive trials were identical. The movement of the animal in the startle chamber was measured for 100 ms after the onset of startle stimulus onset (sampling frequency 1 kHz), rectified, amplified and processed by a computer, which calculated the maximal response over the 100-ms period. Basal startle amplitude was determined as the mean amplitude of the 10 startle trials. PPI (%) was calculated as follows: 100 × (pulse-alone response − prepulse-pulse response)/pulse-alone response, in which prepulse-pulse response was the mean of the 10 PPI trials (20 or 25 ms) and pulse-alone response was the basal startle amplitude.

2.11.9 Y-maze test

The Y-maze apparatus consists of three equal-sized plywood arms (50 cm long, 12 cm high, and 4 cm wide). Each arm of the Y-maze was positioned at an equal angle. Each mouse was placed at the cross points of arms and allowed to move freely through the maze for an 8-min session under moderately light conditions (35 lux). The movement of mice was recorded with a camera mounted above the apparatus. The number of arm entries was counted manually. Spontaneous alternation behavior was defined as the entry into all three arms (i.e., arm A, arm B, and arm C) on consecutive choices in triplet set (i.e., ABC, ACB, BAC, BCA, CAB, and CBA). The percentage of spontaneous alternation behavior was calculated as the ratio of actual to possible alternations (defined as the total number of arm entries − 2) × 100. The Y-maze apparatus was cleaned with 70% ethanol and wiped with paper towels between each trial.

2.11.10 Novel object recognition test

The arena used for the test was an open box (30 cm × 30 cm × 35 cm) covered with fresh bedding. The test procedure consists of three sessions: habituation, training, and retention. During the

habituation session, mice were individually habituated to the open box, in the absence of objects with 10 min of free exploration period for 3 consecutive days. In the training session, two novel objects of similar size, but different shape and color, were placed in the arena and the animals were allowed to explore for 10 min under moderately light conditions (15 lux). Time spent exploring each object was recorded. In the retention session, the animals were placed back into the same box 24 h after the training session, one of the familiar objects used during training was replaced by a novel object, and the mice were allowed to explore freely for 5 min. The preference index in the retention session, the ratio of the amount of time spent exploring the novel object over the total time spent exploring both objects, was used to measure cognitive function. In the training session, the preference index was calculated as the ratio of time spent exploring the replaced novel objects to the total exploration time.

2.11.11 Contextual and cued fear-conditioning test

The fear-conditioning test was conducted using ImageJ FZ1 (O'Hara & Co., Ltd., Tokyo, Japan). The conditioning chamber was a square arena (10 cm × 10 cm × 10 cm) with clear Plexiglas walls and a metal grid floor connected to a circuit board that delivered electric shocks to the metal grid. A video camera was set in front of the cage to record the behavior. In the conditioning session, mice were individually placed into the conditioning chamber and allowed to explore freely at 3 min. After 3 min exploratory period, each mouse was exposed to two tone-footshock pairings (tone, 30 sec; footshock, 2 sec, 0.8 mA at the termination of the tone; separated by 1 min intertrial interval). One min after the second footshock, the mouse was returned to its home cage. 24 h after conditioning, the context-dependent test was performed, in which each mouse was placed back into the conditioning chamber, and the freezing response was measured for 6 min in the absence of the conditioned stimulus. 48 h after the footshock, each mouse was tested for auditory (tone)

fear-conditioning in a novel opaque chamber. Different environmental cues (e.g. light condition and background noise) were provided in the novel chamber. Mice were tested in the novel chamber for a 3 min baseline period (pre-tone) followed by another 3 min for the conditioning tone during which the tone was presented persistently for 3 min. Total freezing rate was measured as an index of fear memory. Motionless bouts lasting more than 2 s were considered as freeze.

2.11.12 Touchscreen-based visual discrimination (VD) and reversal learning

Behavioral training was performed using the touchscreen chamber system (Phenosys, Berlin, Germany; Brain science Idea, Osaka, Japan). The touch screen monitor (5 × 4 inch) was on the front of the chamber and covered by a black plastic mask with 2 response windows (40 × 40 mm^2) to prevent accidental touches. The nozzle for reward delivery was located on the opposite side of the touchscreen monitor. A reward was delivered via the nozzle using a peristaltic pump through a plastic window in the wall. The operant arena (5 cm × 18 cm × 20 cm × 20 cm) consisted of a perforated metal gird floor enclosed by 2 black plastic trapezoidal walls toward to the screen. The operant chamber was placed inside a sound- and light- attenuating box equipped with a fan to provide ventilation and mask background noise. The top of the chamber was covered with a transparent plastic lid.

The battery touchscreen-based behavioral tasks were started with food and water restrictions to motivate mice to perform the task. Food and water restrictions were maintained throughout the touchscreen tasks, and the body weight of test mice was maintained at 85–90% of unrestricted animals. The pre-training includes habituation, initial touch, must touch, must initiate and punish correct. The criterion for successful learning was defined as 75% of correct responses for 2 consecutive sessions in pre-training.

In VD task, a pair of stimuli was presented simultaneously on the screen of pseudorandom

locations. Touching the correct stimulus resulted in a milk liquid reward, touching the incorrect response resulted in a 5-second time out punishment followed by a correction trial. In the correction trials, the pair of stimuli was repeatedly presented on the same screen until the mice make a correct response. The session finishes 60 min or 30 after trials are completed, whichever comes first. The total number of trials, correction trials and correction errors as well as the percentage of correct responses and the perseveration index (the average of sequential correction errors) in different training stages were evaluated. The criterion for successful learning of the VD task was defined as more than 80% of correct responses for 2 consecutive sessions.

The reversal learning in similar to the VD task described above, except that the correct and incorrect stimuli for reward were reversed. The criterion for successful learning of reversal learning was defined as more than 80% of correct responses for 2 consecutive days or completion of 20 sessions.

2.12 Electrophysiology

300-μm-thick prefrontal coronal slices were prepared from 2-week-old mice in the following cutting solution; 120 mM Choline Cl, 28 mM $NaHCO_3$, 1.25 mM NaH_2PO_4, 2 mM KCl, 25 mM glucose, 1 mM $CaCl_2$, 8 mM $MgCl_2$, bubbled with 95 % O_2 and 5 % CO_2 with a vibratome slicer (Leica). The slices were incubated at room temperature for 30–45 min with artificial cerebrospinal fluid (ACSF) composed of 125 mM NaCl, 2.5 mM KCl, 2 mM $CaCl_2$, 1 mM $MgSO_4$, 1.25 mM NaH_2PO_4, 26 mM $NaHCO_3$, and 20 mM glucose bubbled with 95 % O_2 and 5 % CO_2.

In the whole cell patch clamp recording, pyramidal neurons were identified in layer 2/3 of medial prefrontal cortex (mPFC) morphologically. The pipet resistance was 2.4-5 MΩ and it was filled with internal solution of 130 mM K D-gluconate, 6 mM KCl, 10 mM NaCl, 10 mM HEPES, 0.16 mM $CaCl_2$, 2 mM $MgCl_2$, 0.5 mM EGTA, 4 mM ATP, and 0.4 mM GTP (pH 7.3, adjusted

with KOH) for miniature excitatory postsynaptic current (mEPSC). For miniature inhibitory postsynaptic current (mIPSC), the recording pipettes were filled with the following internal solution: 145 mM KCl, 10 mM HEPES, 10 mM EGTA, 0.16 mM $CaCl_2$, 2 mM $MgCl_2$, 5 mM ATP, and 0.2 mM GTP (pH 7.2, adjusted with KOH). All of the recordings were performed at 30–32°C with EPC-10 amplifier (HEKA Elektronik, Lambrecht/Pfalz, Germany). The data was filtered at 2.9 kHz and digitized at 20 kHz. An access resistance of the recording pipettes was compensated by 70 % in the recording. The miniature synaptic responses were recorded at −70 mV in the presence of 0.5 μM tetrodotoxin (TTX) (Nacalai Tesque, Nagoya, Japan) with 0.1 mM picrotoxin (mEPSC) or 10 μM NBQX, 50 μM D-AP5 (mIPSC). Each synaptic response was detected by Mini Analysis program (Synaptosoft Inc., GA, USA) with eyes using the following criteria; over 5 pA, rise time < 3 ms. All of the experiments were performed without information about the genotypes.

2.13 Visual evoked potentials

Visual evoked potentials were recorded from 11-week-old WT (n = 8) and *Del(3.0Mb)/+* mice (n = 7). Under pentobarbital anesthesia (40–50 mg/kg, i.p.), a recording electrode (polyurethane-coated stainless-steel wire with 100 μm in diameter) was chronically implanted into the left visual cortex (2.2 mm lateral, 4.0 mm posterior to bregma, 400 μm ventral to the dura mater). A gold plating pin was positioned in the right frontal bone (0.5 mm lateral, 3.0 mm anterior to bregma) as a reference electrode. Electrodes and a stainless frame for awake head-fixed recording (12 mm × 19 mm, CF-10, Narishige Co. Ltd., Tokyo, Japan) were fixed to the skull with dental acrylic cement.

Visual stimuli were generated and given according to the previous report (Hamm and Yuste, 2016). Briefly, I presented static full-field square-wave grating (100% contrast, 0.04

cycles/degree) on a monitor positioned 15 cm away from the right eye, roughly at 45° to the long axis of the animal. Stimuli were displayed for 500 ms, followed by an interstimulus interval of 1,000 ms of mean luminescence gray screen. A session was composed of 600 stimuli and lasted 15 min.

Four to five days after the implantation, LFP of the left visual cortex was recorded in head-fixed mice at sampling rate of 4 kHz with a 50-Hz hum filter. Signals were amplified (MEG1200, Nihon-koden, Tokyo, Japan) and digitized (PowerLab, AD instruments, Dunedin, New Zealand) for analysis. LFP data were processed using MATLAB. The data were resampled at frequency of 250 Hz and prescreened for excessive artifact (e.g. signal greater than 5 SDs).

2.14 Behavioral rhythm measurement

Male *Del(3.0Mb)/+* mice (n = 14) and WT mice (n = 13) were housed in a polycarbonate cage at the age of 13–16 weeks. They were individually kept in a light-tight (light intensity in the light phase 300 lux) and sound-proof activity recording cage. The spontaneous locomotor activity was measured every min by an infrared thermal sensor. Free-running period was monitored under constant darkness (DD) condition after acclimation in 12-h light/12-h dark cycle (LD) for about 2 weeks. Behavioral activity rhythms were analyzed by Clock Lab (Actimetrics, IL, USA). The circadian period of the activity rhythm under the DD condition was determined by a χ^2 periodogram. For light pulse experiments, mice were first acclimated to LD condition at least 2 weeks and then released into DD condition. Ten to fourteen days after starting DD condition, they were exposed to a single light pulse (30 min, 300 lux) in the early or late subjective night phase at circadian time (CT) 14 or 22, respectively. Phase-shifts were calculated by calculating the phase difference between the two regression lines, one fitted to 10 consecutive activity onsets immediately before the light pulse and the other to those after the light pulse excluding transient

periods of 5 days. For jet lag experiments, mice were acclimated to the LD cycle at least 2 weeks, and then the phase of the LD cycle was advanced or delayed by 8 h.

2.15 Statistical analyses

The significance of differences ($p < 0.05$) was assessed using the two-tailed Welch's *t*-test for comparisons of two groups. In multiple comparisons, the significance of differences was evaluated using an analysis of variance (ANOVA) with two-way repeated measures and Sidak's multiple comparison *post-hoc* test. All data are expressed as the mean ± standard error of the mean (SEM). I decided the sampling size (n) according to the same type of experiments in the previous reports (Nilsson et al., 2016; Stark et al., 2008). The detailed statistics were described at Table 4.

Chapter 3. Results

3.1 Generation of 22q11.2DS mouse model with a 3.0-Mb deletion

Human chromosome 22q11.2 has a conserved linkage group on mouse chromosome 16 (Figure 2). To generate a mouse with a deletion that corresponds to the most common 3.0-Mb deletion in 22q11.2DS patients, I conducted chromosome rearrangement in C57BL/6N mouse zygotes using CRISPR/Cas9 system and single-stranded oligodeoxyribonucleotides (ssODN) as described previously (Boroviak et al., 2016). I designed a pair of single-guide RNAs (sgRNAs) on each target locus of *Pi4ka* intron 47 or *Hira* intron 23 and ssODNs to bridge two Cas9 cleavage sites directly (Figure 4A). Then, four sgRNAs, *hCas9* mRNA and ssODNs were co-injected into the cytoplasm of 1,119 C57BL/6N zygotes, subsequently transplanted 644 viable 2-cell embryos into recipient ICR female mice. Ninety-five pups were obtained from recipient mice and 74 live mice were weaned. To screen a mouse carrying the desired genetic modifications, I performed PCR assay and confirmed the deletion by subsequent direct sequencing of the PCR product. Four pups harbored desired structural variants (Figure 4B, 4D). The efficiency of generating desired mutants was shown in Table 5. I used founder 2 to establish a mutant line (hereafter, referred to as "*Del(3.0Mb)/+*"). The deletion allele of the founder mouse was successfully transmitted through the germline (Figure 4C). The expected decrease in genomic copy number of this region was confirmed in array based comparative genomic hybridization (array CGH) (Figure 4E).

3.2 Gene expression analysis in the brain of *Del(3.0Mb)/+* mice

To identify the molecular changes in the brain of *Del(3.0Mb)/+* mice, I employed gene expression microarray analysis of the hippocampus and the frontal cortex of *Del(3.0Mb)/+* and WT mice. I found 47 probe-sets (~31 genes) in the hippocampus and 54 probe-sets (~34 genes) in the frontal cortex being differentially expressed with false discovery rate (FDR)-corrected *t*-test *P*-value <

0.05 in *Del(3.0Mb)/+* mice (Figure 5A, 5B), and most of them were downregulated in *Del(3.0Mb)/+* mice. Quantitative RT-PCR confirmed that expression of all genes except for *Dgcr8* in the deleted region were significantly reduced to approximately 50% of the expression in WT mice (Figure 5C). *Dgcr8* expression was only reduced to 73.6%, possibly due to negative feedback regulation by the Microprocessor complex containing DGCR8 itself (Triboulet et al., 2009).

Because *Dgcr8* encodes a subunit of the Microprocessor complex required for processing primary miRNA transcripts to mature miRNA, I speculated that expression levels of miRNAs were decreased. A microarray analysis of miRNA revealed that the distribution of the miRNA expression was shifted to the left (Figure 6A, 6B), indicating that miRNA biogenesis was globally downregulated. Specifically, miR-185 showed the largest decrease both in the hippocampus and the frontal cortex of *Del(3.0Mb)/+* mice possibly because miR-185 is located in the deleted region (Figure 6A, 6B). It is notable that a miR-185 target *Emc10* was upregulated in the frontal cortex of *Del(3.0Mb)/+* mice (Figure 5A, 5B). Furthermore, most of the other upregulated genes in hippocampus and frontal cortex (e.g. *Lincppara* and *Spaca6*) were miRNA genes that encode primary miRNAs, indicating accumulation of substrate of the Microprocessor complex.

3.3 Observation of cardiovascular and thymic abnormalities in *Del(3.0Mb)/+* mice

I found that neonatal mortality rate was higher in *Del(3.0Mb)/+* mice than that in WT siblings. Of 211 *Del(3.0Mb)/+* pups, 149 (70.6%) died after birth while 77 (29.1%) out of 265 WT siblings died (Table 6). Cardiac defects are observed in ~80% of the 22q11.2DS patients (Bassett et al., 2005; Goldberg et al., 1993; Ryan et al., 1997) and in *Df1/+* and *Lgdel/+* mice which are 22q11.2DS mouse models (Lindsay et al., 1999; Lindsay et al., 2001; Merscher et al., 2001). In addition to cardiac defects, absence or hypoplasia of the thymus are observed in 22q11.2DS

patients (Markert et al., 1998; Muller et al., 1988; Ryan et al., 1997) and *Df1/+* mice (Taddei et al., 2001). As the higher neonatal mortality rate of *Del(3.0Mb)/+* mice indicated that they had cardiovascular phenotype, I examined embryos at E18.5. Among a total of 33 embryos (15 *Del(3.0Mb)/+* embryos and 18 WT embryos) analyzed, 3 *Del(3.0Mb)/+* embryos had cardiovascular abnormalities. Two embryos (13.3%) had interrupted aortic arch (IAA) and one embryo (6.7%) had aberrant right subclavian artery (ARSA) (Figure 7B, 7D). Seven *Del(3.0Mb)/+* embryos (46.7%) had hypoplasia of the thymus with an asymmetric appearance (Figure 7F). These abnormalities specifically occurred in the mutants and no abnormalities were observed in WT littermates (Figure 7A, 7C, 7E). Penetrance of these defects is summarized in Table 7.

3.4 General locomotor activity and anxiety-like behavior in *Del(3.0Mb)/+* mice

Several studies have characterized behavioral phenotypes of the 22q11.2DS models (Table 1), and I conducted comparable behavioral tests to the previous reports. To evaluate a general locomotor activity, exploration activity and anxiety-like behavior of *Del(3.0Mb)/+* mice, I first performed an open field test (Figure 8A). The total distance of the movement by *Del(3.0Mb)/+* mice was significantly shorter than that by WT mice (Figure 8B). Additionally, *Del(3.0Mb)/+* mice crossed the border between the outer and inner zone less frequently than WT mice (Figure 8C). Meanwhile, there was no significant differences in zone preference (Figure 8D).

I also measured a long-term locomotor activity in a novel home cage for 120 min and observed no significant difference between *Del(3.0Mb)/+* and WT mice (Figure 9A, 9B). However, activity for the first 5 min appeared to be less in *Del(3.0Mb)/+* mice as compared to WT control (Figure 9B). Because the previous 22q11.2DS models showed hyperactivity (Table 1), this hypoactivity phenotype was unique to my model.

Moreover, to evaluate motor functions of *Del(3.0Mb)/+* mice, I conducted the rotarod test, which has been used to assess motor coordination and motor skill learning (Figure 10A). There was no significant difference in the riding time of the rotating rod between *Del(3.0Mb)/+* and WT mice (Figure 10B), indicating that motor coordination and learning of *Del(3.0Mb)/+* mice are normal.

To assess anxiety-like behavior in more detail, I performed an elevated plus maze test (Figure 11A). There was no significant difference in the duration in closed arm or open arm between two genotypes (Figure 11B, 11C), indicating the normal anxiety-like behavior in *Del(3.0Mb)/+* mice, which is consistent with previous reports (Table 1).

3.5 Social behavior in *Del(3.0Mb)/+* mice

Next, I evaluated sociability and social novelty preference by the three-chamber social interaction test. In this test, the subject mouse is first introduced to a novel stranger mouse to assess sociability and subsequently presented to a second novel stranger to evaluate social memory (Figure 12A, 12B). There was no significant difference between *Del(3.0Mb)/+* and WT mice in the sociability and social novelty preference (Figure 12C, 12D).

Because the three-chamber test does not evaluate genuine social memory, I performed a more stringent test, the five-trial direct social interaction test. In this test, a subject mouse was exposed to the same intruder mouse for four successive trials (trial 1–4, Figure 13A). On the fifth trial, the subject mouse was exposed to a novel intruder mouse (trial 5, Figure 13A). Previous reports performing a similar test showed that *Df(16)A*$^{+/-}$ mice had an impaired social memory (Diamantopoulou et al., 2017; Piskorowski et al., 2016). Unlike the previous reports, there was no significant difference in trial 1–4 between two groups but *Del(3.0Mb)/+* mice exhibited significant reduction of the interaction time in trial 5, as compared to WT littermates (Figure 13B).

3.6 Sensorimotor gating in *Del(3.0Mb)/+* mice

Sensorimotor gating is the neurological filtering function to suppress redundant or unnecessary sensory information in the brain, and it is affected in individuals with schizophrenia. Prepulse inhibition (PPI) is one of the well-known translatable measures of sensorimotor gating; patients with schizophrenia (Braff et al., 1999; Grillon et al., 1992; Moriwaki et al., 2009; Parwani et al., 2000) and the 22q11.2DS mouse models have shown reduced PPI (Table 1). To assess the efficiency of sensorimotor gating in *Del(3.0Mb)/+* mice, I evaluated PPI in accordance with a conventional protocol using auditory prepulse stimuli (Figure 14A). As expected, PPI was significantly decreased in *Del(3.0Mb)/+* mice compared to WT controls (Figure 14B). However, the amplitude of startle response *per se* was significantly higher in *Del(3.0Mb)/+* mice than those of WT littermates (Figure 14C). These results were consistent with previous reports (Table 1).

PPI occurs when stimulation of a different modality is applied as a prepulse (Campeau and Davis, 1995; Young et al., 2010). Therefore, I conducted another PPI test using light stimulation as a prepulse (Figure 15A). Both *Del(3.0Mb)/+* and WT mice showed PPI in this paradigm and there was no difference between them (Figure 15B), raising a possibility that reduction of the auditory prepulse-mediated PPI in *Del(3.0Mb)/+* and possibly in the other 22q11.2DS models, was caused by secondary effects of hearing impairments (see Discussion).

3.7 Cognitive function in *Del(3.0Mb)/+* mice

As cognitive dysfunction is common in patients with schizophrenia, I first examined spatial working memory of *Del(3.0Mb)/+* mice by a Y-maze test. Spontaneous alternation behavior, an indicator of spatial working memory, can be evaluated by allowing mice to explore all three arms of the maze (Figure 16A). This behavior is driven by an innate curiosity of animals to explore a new arm. Therefore, a rodent, which has normal spatial working memory, typically prefers to

explore an unvisited arm of the maze rather than returning to previously visited arm. Although the number of mice entering arms and spontaneous alternation were significantly smaller in *Del(3.0Mb)/+* mice as compared to WT controls (Figure 16B, 16C), there was no significant difference in the rate of spontaneous alternation, an indicator of spatial working memory (Figure 16D).

Next, to examine visual cognitive function, particularly recognition memory, I performed a novel object recognition test (Figure 17A). In this experiment, mice are exposed to two different objects, and after 24 h, one of the objects is replaced by a novel object. Typically, when mice are exposed to a familiar and a novel object, they approach frequently and spend more time exploring the novel object than the familiar one. Recognition memory is assessed by the ratio of exploration time for familiar and novel object. There was no significant difference in exploration time and preference between familiar and novel object (Figure 17B, 17C). The reported behavioral data of previous 22q11.2DS models in this test is consistent with our result (Table 1).

To assess associative learning and memory in *Del(3.0Mb)/+* mice, I conducted the pavlovian fear-conditioning test (Figure 18A). In this test, the ability of mice to learn and remember an association between aversive experiences and environmental cues is evaluated using the freezing reaction as an indicator of fear memory recall. This test has repeatedly revealed an impairment of learning and memory in 22q11.2DS models; however, the results were still controversial (Table 1). *Del(3.0Mb)/+* mice showed a decreased freezing time in cue-dependent fear-conditioning test, but the freezing time in contextual fear-conditioning test was not significantly different between two genotypes (Figure 18B).

To evaluate higher cognitive functions *Del(3.0Mb)/+* mice, touchscreen-based visual discrimination (VD) learning and reversal learning tasks were conducted (Figure 19A). The VD task can assess an associative learning between visual images and rewards, working memory and

executive function of mice, and reversal learning task can evaluate behavioral and cognitive flexibility. In the pre-training session, mice were trained to touch a plain white square stimulus to obtain a reward (Figure 19A). There was no significant difference in the number of trials to reach the pre-training criterion (more than 75% correct response for 2 consecutive days) between *Del(3.0Mb)/+* mice and WT mice (Figure 19B). The animals were subsequently subjected to the VD task, in which mice were required to touch a stimulus to obtain a reward from a pair of visual stimuli, marble and fan (Figure 19A). *Del(3.0Mb)/+* mice took an approximately half of the number of total training trials that required for WT mice to reach the criterion (more than 80% correct response for 2 consecutive days) (Figure 19C). The learning curve of the VD task in *Del(3.0Mb)/+* mice was significantly shifted leftward as compared to that of WT mice (Figure 19D). After both groups of mice reached the learning criterion of the VD task, the reward contingencies were reversed (reversal learning task) (Figure 19A). There was no significant difference in the correct response rate (Figure 19E) or perseveration index (Figure 19F) between the genotypes. In line with this, the basal synaptic transmission of layer 2/3 pyramidal neurons in the medial prefrontal cortex (mPFC), a region that is thought to be important for reversal learning, was evaluated. There was no significant difference in amplitude and frequency of miniature excitatory postsynaptic currents (mEPSCs) and miniature inhibitory postsynaptic currents (mIPSCs) between the genotyped (Figure 20A–D), indicating the basal synaptic transmission in the mPFC was normal in *Del(3.0Mb)/+* mice.

3.8 Visual evoked potentials (VEP) in *Del(3.0Mb)/+* mice

Because impairment in early visual sensor processing has been reported in individuals with schizophrenia and their first relatives, I investigated visual evoked potentials (VEP) of *Del(3.0Mb)/+* mice. I recorded local field potentials (LFP) from the primary visual cortex (V1)

area of awake mice, while they are exposed to visual stimuli of square wave gratings (Figure 21A, 21B). VEP responses occurred at the start (ON response) and the end of the stimulus (OFF response) (Figure 21C). In the ON response, peaks of the N1, P1 and N2 components appeared at ~50 ms, ~120 ms and ~ 190 ms from the onset of the stimulus, respectively (Figure 21C). The polarity and latency of the components were similar to those observed in humans (Lascano et al., 2017). I observed generally smaller VEP in *Del(3.0Mb)/+* mice than in WT littermates (Figure 21C). The amplitudes of P1 and N2 peaks were significantly smaller in *Del(3.0Mb)/+* mice (Figure 21D). The latency of each peak (N1, P1 and N2) was not significantly different between two genotypes (Figure 21E).

3.9 Circadian behavioral rhythm in *Del(3.0Mb)/+* mice

Sleep problems are common in patients with 22q11.2DS and psychiatric disorders (Crockett et al., 2014; Heike et al., 2007; Kennedy et al., 2014; Sutton, 2014). A substantial portion of individuals with 22q11.2DS complain of not sleeping well due to obstructive sleep apnea while some patients have difficulties in falling asleep at bedtime. On the other hand, disturbances in circadian rhythm have been implicated in various psychiatric disorders (Charrier et al., 2017). Therefore, circadian rhythm of *Del(3.0Mb)/+* mice was investigated. A χ^2 periodogram analysis of their spontaneous locomotor rhythm in a constant darkness (DD) condition revealed that the free-running period was unaltered in *Del(3.0Mb)/+* mice (Figure 22A). The vulnerability of sleep-wake cycle to the ambient light condition was assessed by light pulse and jet lag tests. In the light pulse test, animals were first entrained to 12 h: 12 h light-dark (LD) cycles for at least 2 weeks and then reared in DD for one day, and in the next day, they were exposed to a 30-min light pulse in the early or late subjective night (CT14 or CT22; CT, circadian time). The resulting phase shift of *Del(3.0Mb)/+* mice after the light exposure was comparable with that of WT controls

(Figure 22B). In the jet lag test, animals were entrained to the LD cycles for at least 2 weeks, and then the phase of the light-dark cycle was advanced or delayed by 8 h. *Del(3.0Mb)/+* mice adapted to a new light-dark cycle faster than WT controls when the phase was advanced (Figure 22C). These results demonstrated that *Del(3.0Mb)/+* mice were more sensitive to an environmental light condition than WT controls, or alternatively that the robustness of the circadian clockwork is reduced in the mutant.

Furthermore, I found that activity levels were significantly reduced in *Del(3.0Mb)/+* mice at around CT16 in DD (Figure 22D), resulting in an emergence of a third peak (previously termed as a night peak, N; see Kon et al., 2014) between the evening (E) and morning (M) peaks (Figure 22D). In LD, on the other hand, the night peak was not as obvious as in DD and temporal activity profile was similar between *Del(3.0Mb)/+* and WT mice (Figure 22E). These observations indicate that an intrinsic circadian rhythm was disturbed in *Del(3.0Mb)/+* mice, but light-induced entrainment can adjust the disturbed behavioral rhythm in the mutant mice.

Chapter 4. Discussion

In the present study, I have generated a novel 22q11.2DS mouse model, *Del(3.0Mb)/+* mice, by using CRISPR/Cas9 system in C57BL/6N genetic background. Our model has significant advantages, because *Del(3.0Mb)/+* mice reproduced the 3.0-Mb deletion that approximately 90% of patients have while the other existing models only mimic a minor 1.5-Mb deletion (Lindsay et al., 1999; Lindsay et al., 2001; Merscher et al., 2001; Nilsson et al., 2016; Stark et al., 2008). I have not investigated whether CRISPR/Cas9 mediated off-target mutations were introduced in the untargeted genomic loci. Therefore, there is a possibility that these phenotypes are influenced by unintended mutations, although potential off-target sites for sgRNAs in this study are located in the intergenic regions or introns (Table 8 and Table 9).

It has been reported that the 1.5-Mb deleted region contains key genes responsible for the increased risk of mental disorders. In fact, some genes within the 1.5-Mb region (e.g. *Tbx1*, *Dgcr8*, *Prodh* and *Sept5*) have been identified as potentially associated with phenotypes relevant to psychiatric disorders by animal model studies (Hiroi and Yamauchi, 2019). On the other hand, the role of the genes existing in the region deleted only in *Del(3.0Mb)/+* model (1.4-Mb region) in psychiatric symptoms of 22q11.2DS is unclear.

A characteristic difference between *Del(3.0Mb)/+* mice and the other 22q11.2DS models is hypoactive: while *Df(16)A*$^{+/-}$ and *Lgdel/+* mice were more active than WT controls in the open field test (Diamantopoulou et al., 2017; Marissal et al., 2018; Stark et al., 2008), *Del(3.0Mb)/+* mice travelled shorter distance. Also, *Del(3.0Mb)/+* mice entered arms less frequently in the Y-maze test, and circadian rhythm analysis revealed that *Del(3.0Mb)/+* mice showed lower activity in their subjective night. This hypoactive phenotype of *Del(3.0Mb)/+* model may reproduce instant fatigability, a frequent complaint among patients with 22q11.2DS (Vergaelen et al., 2017), or negative symptoms of schizophrenia. These results suggest that the 1.4-Mb region contains

genes causing the hypoactivity of the disease.

The impairment of basal social interaction or facial recognition has been observed in individuals with 22q11.2DS (Badoud et al., 2017; Campbell et al., 2010; Campbell et al., 2011; Guo et al., 2018; Jalbrzikowski et al., 2012; Shashi et al., 2012). In the genuine social interaction test, *Del(3.0Mb)/+* mice showed deficit in social recognition of a novel mouse. This phenotype of *Del(3.0Mb)/+* mice probably reproduces the impairment of social recognition observed in 22q11.2DS patients. Meanwhile, social memory of *Del(3.0Mb)/+* mice was intact (Figure 13B; trial 1–4). This result is inconsistent with the social memory impairment of $Df(16)A^{+/-}$ mice shown in previous studies, which conducted direct interaction test (Diamantopoulou et al., 2017; Piskorowski et al., 2016). The contradiction in social behavior between *Del(3.0Mb)/+* and $Df(16)A^{+/-}$ mice may arise from the difference of the genetic background (Table 1). *Del(3.0Mb)/+* mice are pure C57BL/6N genetic background, while $Df(16)A^{+/-}$ mice were hybrid between 129S7/SvEvBrd-$Hprt^{b\text{-}m2}$ and C57BL/6J. Because mice do not replicate all human social cognition, further studies are necessary to clarify correlation between these phenotypes and human counterparts.

Reduction in PPI is a well-known endophenotype of schizophrenia and has been consistently reported in other 22q11.2DS mouse models (Table 1). In the present study, a reduction in PPI was observed when auditory prepulse stimulations were used, but PPI was preserved when light was presented as prepulse. This result argues against the conserved sensorimotor deficit in 22q11.2DS models. One possible explanation of the discrepancy between the prepulse modalities is that *Del(3.0Mb)/+* mice might have a hearing abnormality. Chronic otitis media is a frequent complaint among 22q11.2DS patients (Reyes et al., 1999) and was suggested to cause a hearing difficulty in *Df1/+* mice (Fuchs et al., 2013). Therefore, the reduction in auditory prepulse-mediated PPI in *Del(3.0Mb)/+* mice might be caused by a hearing deficit of tiny prepulse sounds

rather than sensorimotor gating impairment, as suggested in a previous report (Fuchs et al., 2013). Furthermore, it has recently been reported that an increase in acoustic startle response (ASR) correlates with PPI reduction in human and mouse (Csomor et al., 2008; Shoji and Miyakawa, 2018; Yee et al., 2005). Thus, the PPI reduction might be due to the increased ASR in *Del(3.0Mb)/+* mice, making it difficult to interpret the result of PPI analysis. Altogether, *Del(3.0Mb)/+* mice apparently reproduced the sensorimotor deficit of schizophrenia patients but further analyses are required to reveal what caused the PPI reduction in my model.

In the Y-maze test and the VD test, I observed no apparent cognitive deficits in *Del(3.0Mb)/+* mice. *Del(3.0Mb)/+* mice learned the VD task faster than WT mice. This result is consistent with the previous report using a different mouse model of the 22q11.2DS (Nilsson et al., 2016). Functional compensatory changes may protect mice suffering from main neural molecular effects and profound cognitive impairments (Nilsson et al., 2016). Alternatively, 22q11.2 may encode some molecules that limit VD learning. In contrast, there was no difference in performance of reversal learning task between two groups of mice, suggesting that the behavioral flexibility is intact in *Del(3.0Mb)/+* mice. Taken together, these results suggest that 22q11.2 microdeletion slightly enhances ability of VD learning but not flexibility in mice. The electrophysiological data from layer 2/3 pyramidal neurons in the medial prefrontal cortex of 2-week old *Del(3.0Mb)/+* mice suggest that basic parameters of excitatory and inhibitory synaptic transmission are not affected (Figure 20A–D). Short-term depression (STD) was enhanced whereas short-term potentiation (STP) and long-term potentiation (LTP) were both reduced in $Df(16)A^{+/-}$ mice (Diamantopoulou et al., 2017; Piskorowski et al., 2016). Thus, an interesting future study would be to examine synaptic transmission from layer 2 to layer 5 and also to test STD, STP and LTP at this synapse in *Del(3.0Mb)/+* mice to further investigate possible correlation between changes in synaptic function and abnormal behavior observed in *Del(3.0Mb)/+* mice.

Del(3.0Mb)/+ mice displayed a smaller VEP to the static grating stimulations with a significant decrease in the amplitude of the P1 and N2 components but not N1. Because the N1 component has been shown to reflect the input from the lateral geniculate nucleus to the layer 4 in the mouse primary visual cortex (Vaiceliunaite et al., 2013), my results indicate that the visual thalamocortical circuits were relatively intact in *Del(3.0Mb)/+* mice, which contrasts to the deficit of auditory thalamocortical projection in another 22q11.2DS model (Chun et al., 2014). Meanwhile, the reduced P1 and N2 amplitude suggest impaired interlaminar connectivity. The reduced amplitude of VEP, especially that of the P1 component has been recurrently reported in patients with schizophrenia (Biria et al., 2018; Butler et al., 2007; Butler et al., 2001; Doniger et al., 2002; Foxe et al., 2001; Foxe et al., 2005; Knebel et al., 2011) as well as their clinically unaffected relatives, suggesting this deficit as a genetic marker for this disorder (Yeap et al., 2006). Therefore, the reduced VEP of *Del(3.0Mb)/+* mice strongly suggested its validity as a model of schizophrenia. The deficits in early visual processing of schizophrenia have also been demonstrated by apparent dysfunction in visual sensory-perceptual tasks in patients (Butler et al., 1996; Chen et al., 1999a; Chen et al., 1999b; Green and Nuechterlein, 1999; Schwartz et al., 1999a, b). The faster acquisition of the VD task described above might reflect alterations in visual perceptual processing in *Del(3.0Mb)/+* mice.

Interestingly, the present study revealed an impairment of rhythmic activity as a 22q11.2DS model for the first time. *Del(3.0Mb)/+* mice adapted faster to the experimental jet lag with 8-h advancement. This was consistent with the result of the light pulse test, where the phase advance tended to be greater in *Del(3.0Mb)/+* mice. These results suggest that the circadian rhythm of *Del(3.0Mb)/+* mice is more sensitive to an environmental light condition. It is currently unknown how the fast-circadian clock resetting was achieved in *Del(3.0Mb)/+* mice, but the impairment of miRNA biogenesis might be a candidate mechanism. A number of miRNAs have been identified

to show rhythmic expression under control of the circadian clock, and moreover, they can regulate output of the circadian clock via posttranscriptional regulation of the core molecular clock genes in the suprachiasmatic nucleus (SCN) and in peripheral tissues (for review, see Mehta and Cheng, 2013). The most striking example is miR-132, which has been identified as a negative regulator of photic entrainment of circadian rhythm; that is, knocking-down of the miRNA in the SCN potentiated the light-induced clock resetting (Cheng et al., 2007). Although the expression of miR-132 was not significantly changed in *Del(3.0Mb)/+* cortex and hippocampus, compromised biogenesis of miR-132 as well as other miRNA molecules might occur in other brain regions especially in the SCN, potentially leading to the defect in entrainment of circadian rhythm in *Del(3.0Mb)/+* mice.

Furthermore, *Del(3.0Mb)/+* mice showed a characteristic temporal activity profile with an additional peak (termed night peak) at around CT16 in DD. Previously, CaMKIIαK42R mice, which expressed a kinase-dead mutant of CaMKIIα, have shown a similar daily activity profile (Kon et al., 2014). This is particularly interesting because abnormalities in CaMKII have been found in several psychiatric disorders including schizophrenia. These results opened a new avenue for deciphering the relationship between circadian disruption and psychiatric disorders in 22q11.2DS.

Chapter 5. Conclusion

In the present study, I established a novel animal model of 22q11.2DS with an equivalent deletion to the human 3.0-Mb deletion at the 22q11.2 locus. This mouse model has two advantages: first, this model reproduces the most frequent deletion type seen in 22q11.2DS patients; second, *Del(3.0Mb)/+* mice are maintained on pure C57BL/6N genetic background. Moreover, *Del(3.0Mb)/+* mice shows a series of phenotypes that reflect the symptoms observed in patients with 22q11.2DS and schizophrenia. Hence, it is a useful resource to study pathophysiology of schizophrenia associated with 22q11.2DS.

Acknowledgements

I would like to express my sincerest appreciation to my supervisor, Professor Atsu Aiba, for giving me the opportunity to study in his group and for supervising and encouraging me during the entire course of this work. I would also like to express my deepest gratefulness to Dr. Michinori Koebis for his helpful comments and advice about experimental designs and techniques. I also thank Dr. Kazuki Nakao for his insightful suggestions and technical supports about developmental engineering and reproductive technology.

This study was conducted in collaboration with many scientists. I appreciate Ms. Jingzhu Liao, Dr. Bolati Wulaer, Dr. Taku Nagai and Dr. Kiyofumi Yamada (Nagoya University) for their contribution to performing visual discrimination learning and reversal learning tasks, and especially Dr. Nagai for his helpful advice of behavioral experiments. I am profoundly grateful to Dr. Kimiko Shimizu and Dr. Yoshitaka Fukada (The University of Tokyo) for their contribution to conducting circadian behavioral rhythm analysis. I am grateful to Dr. Itaru Kushima, Dr. Daisuke Mori and Dr. Norio Ozaki (Nagoya University) for their contribution to carrying out array CGH analysis. I would like to thank Dr. Kenichiro Nagahama, Dr. Yuki Sugaya, Dr. Naofumi Uesaka and Dr. Masanobu Kano (The University of Tokyo) for their contributions to performing electrophysiological analysis. I also thank Dr. Kazuaki Maruyama and Dr. Hiroki Kurihara (The University of Tokyo) for their technical advice about histological analysis.

I also thank all present and past members of Aiba's laboratory for their helpful advice, discussion and support. Especially, I thank Dr. Ryoko Kudo, Mr. Motoki Goto, Mr. Daisuke Tanaka, Ms. Moe Tamano and Ms. Erina Kawashima for their contributions to generating and maintaining the mutant mouse lines.

Finally, I would like to thank my family and friends for their warm encouragements and mental supports.

This doctoral dissertation was reproduced from Saito et al., Comprehensive analysis of a novel mouse model of the 22q11.2 deletion syndrome: a model with the most common 3.0-Mb deletion at the human locus. *Translational psychiatry* 10, 35 (2020). https://doi.org/10.1038/s41398-020-0723-z

Ryo Saito

References

Aubert, L., Reiss, D., and Ouagazzal, A.M. (2006). Auditory and visual prepulse inhibition in mice: parametric analysis and strain comparisons. *Genes Brain. Behav.* 5, 423–431.

Badoud, D., Schneider, M., Menghetti, S., Glaser, B., Debbane, M., and Eliez, S. (2017). Understanding others: a pilot investigation of cognitive and affective facets of social cognition in patients with 22q11.2 deletion syndrome (22q11DS). *J. Neurodev. Disord.* 9, 35.

Barrangou, R. (2013). CRISPR-Cas systems and RNA-guided interference. *Wiley Interdiscip. Rev. RNA* 4, 267–278.

Barrangou, R., Fremaux, C., Deveau, H., Richards, M., Boyaval, P., Moineau, S., Romero, D.A., and Horvath, P. (2007). CRISPR provides acquired resistance against viruses in prokaryotes. *Science* 315, 1709–1712.

Bassett, A.S., Chow, E.W., Husted, J., Weksberg, R., Caluseriu, O., Webb, G.D., and Gatzoulis, M.A. (2005). Clinical features of 78 adults with 22q11 deletion syndrome. *Am. J. Med. Genet. A. 138A*, 307–313.

Biria, M., Tomescu, M.I., Custo, A., Cantonas, L.M., Song, K.W., Schneider, M., Murray, M.M., Eliez, S., Michel, C.M., and Rihs, T.A. (2018). Visual processing deficits in 22q11.2 deletion syndrome. *Neuroimage Clin.* 17, 976–986.

Boroviak, K., Doe, B., Banerjee, R., Yang, F., and Bradley, A. (2016). Chromosome engineering in zygotes with CRISPR/Cas9. *Genesis* 54, 78–85.

Botto, L.D., May, K., Fernhoff, P.M., Correa, A., Coleman, K., Rasmussen, S.A., Merritt, R.K., O'Leary, L.A., Wong, L.Y., Elixson, E.M.*, et al*. (2003). A population-based study of the 22q11.2 deletion: phenotype, incidence, and contribution to major birth defects in the population. *Pediatrics* 112, 101–107.

Bradley, A., Evans, M., Kaufman, M.H., and Robertson, E. (1984). Formation of germ-line chimaeras from embryo-derived teratocarcinoma cell lines. *Nature* 309, 255–256.

Braff, D.L., Swerdlow, N.R., and Geyer, M.A. (1999). Symptom correlates of prepulse inhibition

deficits in male schizophrenic patients. *Am. J. Psychiatry* 156, 596–602.

Buckley, E., Siddique, A., and McNeill, A. (2017). Hyposmia, symptoms of rapid eye movement sleep behavior disorder, and parkinsonian motor signs suggest prodromal neurodegeneration in 22q11 deletion syndrome. *Neuroreport* 28, 677–681.

Burnside, R.D. (2015). 22q11.21 deletion syndromes: a review of proximal, central, and distal deletions and their associated features. *Cytogenet. Genome Res.* 146, 89–99.

Butler, P.D., Harkavy-Friedman, J.M., Amador, X.F., and Goman, J.M. (1996). Backward masking in schizophrenia: relationship to medication status, neuropsychological functioning, and dopamine metabolism. *Biol. Psychiatry* 40, 295–298.

Butler, P.D., Martinez, A., Foxe, J.J., Kim, D., Zemon, V., Silipo, G., Mahoney, J., Shpaner, M., Jalbrzikowski, M., and Javitt, D.C. (2007). Subcortical visual dysfunction in schizophrenia drives secondary cortical impairments. *Brain* 130, 417–430.

Butler, P.D., Schechter, I., Zemon, V., Schwartz, S.G., Greenstein, V.C., Gordon, J., Schroeder, C.E., and Javitt, D.C. (2001). Dysfunction of early-stage visual processing in schizophrenia. *Am. J. Psychiatry* 158, 1126–1133.

Campbell, L., McCabe, K., Leadbeater, K., Schall, U., Loughland, C., and Rich, D. (2010). Visual scanning of faces in 22q11.2 deletion syndrome: attention to the mouth or the eyes? *Psychiatry Res.* 177, 211–215.

Campbell, L.E., Stevens, A.F., McCabe, K., Cruickshank, L., Morris, R.G., Murphy, D.G., and Murphy, K.C. (2011). Is theory of mind related to social dysfunction and emotional problems in 22q11.2 deletion syndrome (velo-cardio-facial syndrome)? *J. Neurodev. Disord.* 3, 152–161.

Campeau, S., and Davis, M. (1995). Prepulse inhibition of the acoustic startle reflex using visual and auditory prepulses: disruption by apomorphine. *Psychopharmacology* 117, 267–274.

Cardno, A.G., and Gottesman, II (2000). Twin studies of schizophrenia: From bow-and-arrow concordances to star wars mx and functional genomics. *Am. J. Med. Genet.* 97, 12–17.

Carlson, C., Sirotkin, H., Pandita, R., Goldberg, R., McKie, J., Wadey, R., Patanjali, S.R.,

Weissman, S.M., Anyane-Yeboa, K., Warburton, D., *et al*. (1997). Molecular definition of 22q11 deletions in 151 velo-cardio-facial syndrome patients. *Am. J. Hum. Genet. 61*, 620–629.

Charrier, A., Olliac, B., Roubertoux, P., and Tordjman, S. (2017). Clock genes and altered sleep-wake rhythms: their role in the development of psychiatric disorders. *Int. J. Mol. Sci.* 18, E938.

Chen, Y., Levy, D.L., Nakayama, K., Matthysse, S., Palafox, G., and Holzman, P.S. (1999a). Dependence of impaired eye tracking on deficient velocity discrimination in schizophrenia. *Arch. Gen. Psychiatry* 56, 155–161.

Chen, Y., Nakayama, K., Levy, D.L., Mathysse, S., and Holzman, P.S. (1999b). Psychophysical isolation of a motion-processing deficit in schizophrenics and their relatives and its association with impaired smooth pursuit. *Proc. Natl. Acad. Sci. USA.* 96, 4724–4729.

Cheng, H.Y., Papp, J.W., Varlamova, O., Dziema, H., Russell, B., Curfman, J.P., Nakazawa, T., Shimizu, K., Okamura, H., Impey, S., and Obrietan, K. (2007). microRNA modulation of circadian-clock period and entrainment. *Neuron* 54, 813–829.

Chou, I.J., Kuo, C.F., Huang, Y.S., Grainge, M.J., Valdes, A.M., See, L.C., Yu, K.H., Luo, S.F., Huang, L.S., Tseng, W.Y., *et al*. (2017). Familial aggregation and heritability of schizophrenia and co-aggregation of psychiatric illnesses in affected families. *Schizophr. Bull.* 43, 1070–1078.

Chun, S., Westmoreland, J.J., Bayazitov, I.T., Eddins, D., Pani, A.K., Smeyne, R.J., Yu, J., Blundon, J.A., and Zakharenko, S.S. (2014). Specific disruption of thalamic inputs to the auditory cortex in schizophrenia models. *Science* 344, 1178–1182.

Cong, L., Ran, F.A., Cox, D., Lin, S., Barretto, R., Habib, N., Hsu, P.D., Wu, X., Jiang, W., Marraffini, L.A., *et al*. (2013). Multiplex genome engineering using CRISPR/Cas systems. *Science* 339, 819–823.

Crockett, D.J., Goudy, S.L., Chinnadurai, S., and Wootten, C.T. (2014). Obstructive sleep apnea syndrome in children with 22q11.2 deletion syndrome after operative intervention for velopharyngeal insufficiency. *Front. Pediatr.* 2, 84.

Csomor, P.A., Yee, B.K., Vollenweider, F.X., Feldon, J., Nicolet, T., and Quednow, B.B. (2008). On the influence of baseline startle reactivity on the indexation of prepulse inhibition. *Behav.*

Neurosci. 122, 885–900.

Cunningham, A.C., Delport, S., Cumines, W., Busse, M., Linden, D.E., Hall, J., Owen, M.J., and van den Bree, M.B. (2018). Developmental coordination disorder, psychopathology and IQ in 22q11.2 deletion syndrome. *Br. J. Psychiatry* 212, 27–33.

Debbane, M., Glaser, B., and Eliez, S. (2008). Encoding and retrieval processes in velo-cardio-facial syndrome (VCFS). *Neuropsychology* 22, 226–234.

Devriendt, K., Fryns, J.P., Mortier, G., van Thienen, M.K., and Keymolen, K. (1998). The annual incidence of DiGeorge/velocardiofacial syndrome. *J. Med. Geneti.* 35, 789–790.

Diamantopoulou, A., Sun, Z., Mukai, J., Xu, B., Fenelon, K., Karayiorgou, M., and Gogos, J.A. (2017). Loss-of-function mutation in *Mirta22*/*Emc10* rescues specific schizophrenia-related phenotypes in a mouse model of the 22q11.2 deletion. *Proc. Natl. Acad. Sci. USA.* 114, E6127–E6136.

Doniger, G.M., Foxe, J.J., Murray, M.M., Higgins, B.A., and Javitt, D.C. (2002). Impaired visual object recognition and dorsal/ventral stream interaction in schizophrenia. *Arch. Gen. Psychiatry* 59, 1011–1020.

Edelmann, L., Pandita, R.K., Spiteri, E., Funke, B., Goldberg, R., Palanisamy, N., Chaganti, R.S., Magenis, E., Shprintzen, R.J., and Morrow, B.E. (1999). A common molecular basis for rearrangement disorders on chromosome 22q11. *Hum. Mol. Genet.* 8, 1157–1167.

Emanuel, B.S. (2008). Molecular mechanisms and diagnosis of chromosome 22q11.2 rearrangements. *Dev. Disabil. Res. Rev.* 14, 11–18.

Feuk, L., Carson, A.R. and Scherer, S.W. (2006). Structural variation in the human genome. *Nat. Rev. Genet.* 7, 85–97.

Fine, S.E., Weissman, A., Gerdes, M., Pinto-Martin, J., Zackai, E.H., McDonald-McGinn, D.M., and Emanuel, B.S. (2005). Autism spectrum disorders and symptoms in children with molecularly confirmed 22q11.2 deletion syndrome. *J. Autism. Dev. Disord.* 35, 461–470.

Foxe, J.J., Doniger, G.M., and Javitt, D.C. (2001). Early visual, processing deficits in

schizophrenia: impaired P1 generation revealed by high-density electrical mapping. *Neuroreport* 12, 3815–3820.

Foxe, J.J., Murray, M.M., and Javitt, D.C. (2005). Filling-in in schizophrenia: a high-density electrical mapping and source-analysis investigation of illusory contour processing. *Cereb. Cortex* 15, 1914–1927.

Fuchs, J.C., Zinnamon, F.A., Taylor, R.R., Ivins, S., Scambler, P.J., Forge, A., Tucker, A.S., and Linden, J.F. (2013). Hearing loss in a mouse model of 22q11.2 deletion syndrome. *PLoS One* 8, e80104.

Fung, W.L., McEvilly, R., Fong, J., Silversides, C., Chow, E., Bassett, A. (2010). Elevated prevalence of generalized anxiety disorder in adults with 22q11.2 deletion syndrome. *Am. J. Psychiatry* 167, 998–998.

Gasiunas, G., Barrangou, R., Horvath, P., and Siksnys, V. (2012). Cas9-crRNA ribonucleoprotein complex mediates specific DNA cleavage for adaptive immunity in bacteria. *Proc. Natl. Acad. Sci. USA.* 109, E2579–E2586.

Goldberg, R., Motzkin, B., Marion, R., Scambler, P.J., and Shprintzen, R.J. (1993). Velo-cardio-facial syndrome: a review of 120 patients. *Am. J. Med. Genet.* 45, 313–319.

Gothelf, D., Presburger, G., Zohar, A.H., Burg, M., Nahmani, A., Frydman, M., Shohat, M., Inbar, D., Aviram-Goldring, A., Yeshaya, J., *et al*. (2004). Obsessive-compulsive disorder in patients with velocardiofacial (22q11 deletion) syndrome. *Am. J. Med. Genet. B. Neuropsychiatr. Genet.* 126B, 99–105.

Grati, F.R., Molina Gomes, D., Ferreira, J.C., Dupont, C., Alesi, V., Gouas, L., Horelli-Kuitunen, N., Choy, K.W., Garcia-Herrero, S., de la Vega, A.G., *et al*. (2015). Prevalence of recurrent pathogenic microdeletions and microduplications in over 9500 pregnancies. *Prenat. Diagn.* 35, 801–809.

Green, M.F., and Nuechterlein, K.H. (1999). Backward masking performance as an indicator of vulnerability to schizophrenia. *Acta. Psychiatr. Scand. Suppl.* 395, 34–40.

Grillon, C., Ameli, R., Charney, D.S., Krystal, J., and Braff, D. (1992). Startle gating deficits occur

across prepulse intensities in schizophrenic patients. *Biol. Psychiatry* 32, 939–943.

Grozeva, D., Conrad, D.F., Barnes, C.P., Hurles, M., Owen, M.J., O'Donovan, M.C., Craddock, N., Kirov, G., and WTCCC (2012). Independent estimation of the frequency of rare CNVs in the UK population confirms their role in schizophrenia. *Schizophr. Res.* 135, 1–7.

Guna, A., Butcher, N.J., and Bassett, A.S. (2015). Comparative mapping of the 22q11.2 deletion region and the potential of simple model organisms. *J. Neurodev. Disord.* 7, 18.

Guo, T., Diacou, A., Nomaru, H., McDonald-McGinn, D.M., Hestand, M., Demaerel, W., Zhang, L., Zhao, Y., Ujueta, F., Shan, J., *et al*. (2018). Deletion size analysis of 1680 22q11.2DS subjects identifies a new recombination hotspot on chromosome 22q11.2. *Hum. Mol. Genet.* 27, 1150–1163.

Hamm, J.P., and Yuste, R. (2016). Somatostatin interneurons control a key component of mismatch negativity in mouse visual cortex. *Cell Rep.* 16, 597–604.

Heike, C.L., Avellino, A.M., Mirza, S.K., Kifle, Y., Perkins, J., Sze, R., Egbert, M., and Hing, A.V. (2007). Sleep disturbances in 22q11.2 deletion syndrome: a case with obstructive and central sleep apnea. *Cleft Palate Craniofac. J.* 44, 340–346.

Herault, Y., Rassoulzadegan, M., Cuzin, F., and Duboule, D. (1998). Engineering chromosomes in mice through targeted meiotic recombination (TAMERE). *Nat. Genet.* 20, 381–384.

Hiroi, N. (2018). Critical reappraisal of mechanistic links of copy number variants to dimensional constructs of neuropsychiatric disorders in mouse models. *Psychiatry Clin. Neurosci.* 72, 301–321.

Hiroi, N., and Yamauchi, T. (2019). Modeling and predicting developmental trajectories of neuropsychiatric dimensions associated with copy number variations. *Int. J. neuropsychopharmacol.* 22, 488–500.

International Schizophrenia Consortium. (2009). Common polygenic variation contributes to risk of schizophrenia and bipolar disorder. *Nature* 460, 748–752.

Ishino, Y., Shinagawa, H., Makino, K., Amemura, M., and Nakata, A. (1987). Nucleotide sequence of the iap gene, responsible for alkaline phosphatase isozyme conversion in Escherichia coli, and identification of the gene product. *J. Bacteriol.* 169, 5429–5433.

Jalbrzikowski, M., Carter, C., Senturk, D., Chow, C., Hopkins, J.M., Green, M.F., Galvan, A., Cannon, T.D., and Bearden, C.E. (2012). Social cognition in 22q11.2 microdeletion syndrome: Relevance to psychosis? *Schizophr. Res.* 142, 99–107.

Jansen, R., van Embden, J.D., Gaastra, W., and Schouls, L.M. (2002). Identification of genes that are associated with DNA repeats in prokaryotes. *Mol. Microbiol.* 43, 1565–1575.

Kennedy, W.P., Mudd, P.A., Maguire, M.A., Souders, M.C., McDonald-McGinn, D.M., Marcus, C.L., Zackai, E.H., Solot, C.B., Mason, T.B., Jackson, O.A., *et al*. (2014). 22q11.2 Deletion syndrome and obstructive sleep apnea. *Int. J. Pediatr. Otorhinolaryngol.* 78, 1360–1364.

Kirov, G., Rees, E., Walters, J.T., Escott-Price, V., Georgieva, L., Richards, A.L., Chambert, K.D., Davies, G., Legge, S.E., Moran, J.L., *et al*. (2014). The penetrance of copy number variations for schizophrenia and developmental delay. *Biol. Psychiatry* 75, 378–385.

Knebel, J.F., Javitt, D.C., and Murray, M.M. (2011). Impaired early visual response modulations to spatial information in chronic schizophrenia. *Psychiatry Res.* 193, 168–176.

Kon, N., Yoshikawa, T., Honma, S., Yamagata, Y., Yoshitane, H., Shimizu, K., Sugiyama, Y., Hara, C., Kameshita, I., Honma, K., *et al*. (2014). CaMKII is essential for the cellular clock and coupling between morning and evening behavioral rhythms. *Genes Dev.* 28, 1101–1110.

Kraft, K., Geuer, S., Will, A.J., Chan, W.L., Paliou, C., Borschiwer, M., Harabula, I., Wittler, L., Franke, M., Ibrahim, D.M., *et al*. (2015). Deletions, inversions, duplications: engineering of structural variants using CRISPR/Cas in mice. *Cell Rep.* 10, 833–839.

Kushima, I., Aleksic, B., Nakatochi, M., Shimamura, T., Okada, T., Uno, Y., Morikawa, M., Ishizuka, K., Shiino, T., Kimura, H., *et al*. (2018). Comparative analyses of copy-number variation in autism spectrum disorder and schizophrenia reveal etiological overlap and biological insights. *Cell Rep.* 24, 2838–2856.

Lascano, A.M., Lalive, P.H., Hardmeier, M., Fuhr, P., and Seeck, M. (2017). Clinical evoked potentials in neurology: a review of techniques and indications. *J. Neurol. Neurosurg. Psychiatry* 88, 688–696.

Levinson, D.F., Duan, J., Oh, S., Wang, K., Sanders, A.R., Shi, J., Zhang, N., Mowry, B.J., Olincy, A., Amin, F., *et al*. (2011). Copy number variants in schizophrenia: confirmation of five previous findings and new evidence for 3q29 microdeletions and VIPR2 duplications. *Am. J. Psychiatry* 168, 302–316.

Li, H.H., Roy, M., Kuscuoglu, U., Spencer, C.M., Halm, B., Harrison, K.C., Bayle, J.H., Splendore, A., Ding, F., Meltzer, L.A.*, et al.* (2009). Induced chromosome deletions cause hypersociability and other features of Williams-Beuren syndrome in mice. *EMBO Mol. Med.* 1, 50–65.

Lindsay, E.A., Botta, A., Jurecic, V., Carattini-Rivera, S., Cheah, Y.C., Rosenblatt, H.M., Bradley, A., and Baldini, A. (1999). Congenital heart disease in mice deficient for the DiGeorge syndrome region. *Nature* 401, 379–383.

Lindsay, E.A., Vitelli, F., Su, H., Morishima, M., Huynh, T., Pramparo, T., Jurecic, V., Ogunrinu, G., Sutherland, H.F., Scambler, P.J., *et al*. (2001). Tbx1 haploinsufficiency in the DiGeorge syndrome region causes aortic arch defects in mice. *Nature* 410, 97–101.

Livak, K.J., and Schmittgen, T.D. (2001). Analysis of relative gene expression data using real-time quantitative PCR and the 2 (-Delta Delta C (T)) method. *Methods* 25, 402–408.

Lopez-Rivera, E., Liu, Y.P., Verbitsky, M., Anderson, B.R., Capone, V.P., Otto, E.A., Yan, Z., Mitrotti, A., Martino, J., Steers, N.J., *et al*. (2017). Genetic drivers of kidney defects in the DiGeorge syndrome. *N. Engl. J. Med.* 376, 742–754.

Mali, P., Yang, L., Esvelt, K.M., Aach, J., Guell, M., DiCarlo, J.E., Norville, J.E., and Church, G.M. (2013). RNA-guided human genome engineering via Cas9. *Science* 339, 823–826.

Marissal, T., Salazar, R.F., Bertollini, C., Mutel, S., De Roo, M., Rodriguez, I., Muller, D., and Carleton, A. (2018). Restoring wild-type-like CA1 network dynamics and behavior during adulthood in a mouse model of schizophrenia. *Nat. Neurosci.* 21, 1412–1420.

Markert, M.L., Hummell, D.S., Rosenblatt, H.M., Schiff, S.E., Harville, T.O., Williams, L.W., Schiff, R.I., and Buckley, R.H. (1998). Complete DiGeorge syndrome: persistence of profound immunodeficiency. *J. Pediatr.* 132, 15–21.

McCabe, K.L., Marlin, S., Cooper, G., Morris, R., Schall, U., Murphy, D.G., Murphy, K.C., and Campbell, L.E. (2016). Visual perception and processing in children with 22q11.2 deletion syndrome: associations with social cognition measures of face identity and emotion recognition. *J. Neurodev. Disord.* 8, 30.

Mehta, N., and Cheng, H.Y. (2013). Micro-managing the circadian clock: the role of microRNAs in biological timekeeping. *J. Mol. Biol.* 425, 3609–3624.

Merscher, S., Funke, B., Epstein, J.A., Heyer, J., Puech, A., Lu, M.M., Xavier, R.J., Demay, M.B., Russell, R.G., Factor, S., *et al*. (2001). TBX1 is responsible for cardiovascular defects in velo-cardio-facial/DiGeorge syndrome. *Cell* 104, 619–629.

Michaelovsky, E., Frisch, A., Carmel, M., Patya, M., Zarchi, O., Green, T., Basel-Vanagaite, L., Weizman, A., and Gothelf, D. (2012). Genotype-phenotype correlation in 22q11.2 deletion syndrome. *BMC Med. Genet.* 13, 122.

Mok, K.Y., Sheerin, U., Simon-Sanchez, J., Salaka, A., Chester, L., Escott-Price, V., Mantripragada, K., Doherty, K.M., Noyce, A.J., Mencacci, N.E., *et al*. (2016). Deletions at 22q11.2 in idiopathic Parkinson's disease: a combined analysis of genome-wide association data. *Lancet Neurol.* 15, 585–596.

Moreno-De-Luca, D., Mulle, J.G., Kaminsky, E.B., Sanders, S.J., Myers, S.M., Adam, M.P., Pakula, A.T., Eisenhauer, N.J., Uhas, K., Weik, L., *et al*. (2010). Deletion 17q12 is a recurrent copy number variant that confers high risk of autism and schizophrenia. *Am. J. Hum. Genet.* 87, 618–630.

Moriwaki, M., Kishi, T., Takahashi, H., Hashimoto, R., Kawashima, K., Okochi, T., Kitajima, T., Furukawa, O., Fujita, K., Takeda, M., *et al*. (2009). Prepulse inhibition of the startle response with chronic schizophrenia: a replication study. *Neurosci. Res.* 65, 259–262.

Muller, W., Peter, H.H., Wilken, M., Juppner, H., Kallfelz, H.C., Krohn, H.P., Miller, K., and Rieger, C.H. (1988). The DiGeorge syndrome. 1. Clinical evaluation and course of partial and

complete forms of the syndrome. *Eur. J. Pediatr.* 147, 496–502.

Naito, Y., Hino, K., Bono, H., and Ui-Tei, K. (2015). CRISPRdirect: software for designing CRISPR/Cas guide RNA with reduced off-target sites. *Bioinformatics* 31, 1120–1123.

Nakao, H., Harada, T., Nakao, K., Kiyonari, H., Inoue, K., Furuta, Y., and Aiba, A. (2016). A possible aid in targeted insertion of large DNA elements by CRISPR/Cas in mouse zygotes. *Genesis* 54, 65–77.

Niklasson, L., Rasmussen, P., Oskarsdottir, S., and Gillberg, C. (2009). Autism, ADHD, mental retardation and behavior problems in 100 individuals with 22q11 deletion syndrome. *Res. Dev. Disabil.* 30, 763–773.

Nilsson, S.R., Fejgin, K., Gastambide, F., Vogt, M.A., Kent, B.A., Nielsen, V., Nielsen, J., Gass, P., Robbins, T.W., Saksida, L.M., *et al*. (2016). Assessing the cognitive translational potential of a mouse model of the 22q11.2 microdeletion syndrome. *Cereb. Cortex* 26, 3991–4003.

O'Donovan, M.C., Craddock, N., Norton, N., Williams, H., Peirce, T., Moskvina, V., Nikolov, I., Hamshere, M., Carroll, L., Georgieva, L., *et al*. (2008). Identification of loci associated with schizophrenia by genome-wide association and follow-up. *Nat. Genet.* 40, 1053–1055.

Parwani, A., Duncan, E.J., Bartlett, E., Madonick, S.H., Efferen, T.R., Rajan, R., Sanfilipo, M., Chappell, P.B., Chakravorty, S., Gonzenbach, S., *et al*. (2000). Impaired prepulse inhibition of acoustic startle in schizophrenia. *Biol. Psychiatry* 47, 662–669.

Piskorowski, R.A., Nasrallah, K., Diamantopoulou, A., Mukai, J., Hassan, S.I., Siegelbaum, S.A., Gogos, J.A., and Chevaleyre, V. (2016). Age-dependent specific changes in area CA2 of the hippocampus and social memory deficit in a mouse model of the 22q11.2 deletion syndrome. *Neuron* 89, 163–176.

Puech, A., Saint-Jore, B., Funke, B., Gilbert, D.J., Sirotkin, H., Copeland, N.G., Jenkins, N.A., Kucherlapati, R., Morrow, B., and Skoultchi, A.I. (1997). Comparative mapping of the human 22q11 chromosomal region and the orthologous region in mice reveals complex changes in gene organization. *Proc. Natl. Acad. Sci. USA.* 94, 14608–14613.

Ramirez-Solis, R., Liu, P.T., and Bradley, A. (1995). Chromosome engineering in mice.

Nature 378, 720–724.

Reyes, M.R., LeBlanc, E.M., and Bassila, M.K. (1999). Hearing loss and otitis media in velo-cardio-facial syndrome. *Int. J. Pediatr. Otorhinolaryngol.* 47, 227–233.

Rietschel, M., Mattheisen, M., Degenhardt, F., Muhleisen, T.W., Kirsch, P., Esslinger, C., Herms, S., Demontis, D., Steffens, M., Strohmaier, J., *et al*. (2012). Association between genetic variation in a region on chromosome 11 and schizophrenia in large samples from Europe. *Mol. Psychiatry* 17, 906–917.

Ruf, S., Symmons, O., Uslu, V.V., Dolle, D., Hot, C., Ettwiller, L., and Spitz, F. (2011). Large-scale analysis of the regulatory architecture of the mouse genome with a transposon-associated sensor. *Nat. Genet.* 43, 379–386.

Ryan, A.K., Goodship, J.A., Wilson, D.I., Philip, N., Levy, A., Seidel, H., Schuffenhauer, S., Oechsler, H., Belohradsky, B., Prieur, M., *et al*. (1997). Spectrum of clinical features associated with interstitial chromosome 22q11 deletions: a European collaborative study. *J. Med. Genet.* 34, 798–804.

Schneider, M., Debbané, M, Bassett, A.S., Chow, E.W., Fung, W.L., van den Bree, M., Owen, M., Murphy, K.C., Niarchou, M., Kates, W.R. *et al.* (2014). Psychiatric disorders from childhood to adulthood in 22q11.2 deletion syndrome: results from the international consortium on brain and behavior in 22q11.2 deletion syndrome. *Am. J. Psychiatry* 171, 627–639.

Schwartz, B.D., Maron, B.A., Evans, W.J., and Winstead, D.K. (1999a). High velocity transient visual processing deficits diminish ability of patients with schizophrenia to recognize objects. *Neuropsychiatry Neuropsychol. Behav. Neurol.* 12, 170–177.

Schwartz, B.D., Maron, B.A., Evans, W.J., and Winstead, D.K. (1999b). Smooth pursuit tracking deficits of patients with schizophrenia at specific within-sine wave bins. *Neuropsychiatry Neuropsychol. Behav. Neurol.* 12, 221–229.

Shaikh, T.H., Kurahashi, H., and Emanuel, B.S. (2001). Evolutionarily conserved low copy repeats (LCRs) in 22q11 mediate deletions, duplications, translocations, and genomic instability: an update and literature review. *Genet. Med.* 3, 6–13.

Shapiro, H.M., Tassone, F., Choudhary, N.S., and Simon, T.J. (2014). The development of cognitive control in children with chromosome 22q11.2 deletion syndrome. *Front. Psychol.* 5, 556.

Shashi, V., Veerapandiyan, A., Schoch, K., Kwapil, T., Keshavan, M., Ip, E., and Hooper, S. (2012). Social skills and associated psychopathology in children with chromosome 22q11.2 deletion syndrome: implications for interventions. *J. Intellect. Disabil. Res.* 56, 865–878.

Shi, Y., Li, Z., Xu, Q., Wang, T., Li, T., Shen, J., Zhang, F., Chen, J., Zhou, G., Ji, W., *et al*. (2011). Common variants on 8p12 and 1q24.2 confer risk of schizophrenia. *Nat. Genet.* 43, 1224–1227.

Shoji, H., and Miyakawa, T. (2018). Relationships between the acoustic startle response and prepulse inhibition in C57BL/6J mice: a large-scale meta-analytic study. *Mol. Brain* 11, 42.

Sittig, L.J., Carbonetto, P., Engel, K.A., Krauss, K.S., Barrios-Camacho, C.M., and Palmer, A.A. (2016). Genetic background limits generalizability of genotype-phenotype relationships. *Neuron* 91, 1253–1259.

Smith, A.J., Desousa, M.A., Kwabi-Addo, B., Heppell-Parton, A., Impey, H., and Rabbitts, P. (1995). A site-directed chromosomal translocation induced in embryonic stem cells by Cre-*loxP* recombination. *Nat. Genet.* 9, 376–385.

Sobin, C., Kiley-Brabeck, K., and Karayiorgou, M. (2005a). Lower prepulse inhibition in children with the 22q11 deletion syndrome. *Am. J. Psychiatry* 162, 1090–1099.

Sobin, C., Kiley-Brabeck, K., and Karayiorgou, M. (2005b). Associations between prepulse inhibition and executive visual attention in children with the 22q11 deletion syndrome. *Mol. Psychiatry* 10, 553–562.

Spitz, F., Herkenne, C., Morris, M.A., and Duboule, D. (2005). Inversion-induced disruption of the *Hoxd* cluster leads to the partition of regulatory landscapes. *Nat. Genet. 37*, 889–893.

Stark, K.L., Xu, B., Bagchi, A., Lai, W.S., Liu, H., Hsu, R., Wan, X., Pavlidis, P., Mills, A.A., Karayiorgou, M., *et al*. (2008). Altered brain microRNA biogenesis contributes to phenotypic deficits in a 22q11-deletion mouse model. *Nat. Genet.* 40, 751–760.

Steinberg, S., de Jong, S., Andreassen, O.A., Werge, T., Borglum, A.D., Mors, O., Mortensen, P.B., Gustafsson, O., Costas, J., Pietilainen, O.P., *et al*. (2011). Common variants at VRK2 and TCF4 conferring risk of schizophrenia. *Hum. Mol. Genet.* 20, 4076–4081.

Sutton, E.L. (2014). Psychiatric disorders and sleep issues. *Med. Clin. North Am.* 98, 1123–1143.

Szatkiewicz, J.P., O'Dushlaine, C., Chen, G., Chambert, K., Moran, J.L., Neale, B.M., Fromer, M., Ruderfer, D., Akterin, S., Bergen, S.E., *et al*. (2014). Copy number variation in schizophrenia in Sweden. *Mol. Psychiatry* 19, 762–773.

Taddei, I., Morishima, M., Huynh, T., and Lindsay, E.A. (2001). Genetic factors are major determinants of phenotypic variability in a mouse model of the DiGeorge/del22q11 syndromes. *Proc. Natl. Acad. Sci. USA*. 98, 11428–11431.

The International Schizophrenia Consortium. (2008). Rare chromosomal deletions and duplications increase risk of schizophrenia. *Nature* 455, 237–241.

The Schizophrenia Psychiatric Genome-Wide Association Study Consortium. (2011). Genome-wide association study identifies five new schizophrenia loci. *Nat. Genet.* 43, 969–976.

Triboulet, R., Chang, H.M., Lapierre, R.J., and Gregory, R.I. (2009). Post-transcriptional control of DGCR8 expression by the Microprocessor. *RNA* 15, 1005–1011.

Vacic, V., McCarthy, S., Malhotra, D., Murray, F., Chou, H.H., Peoples, A., Makarov, V., Yoon, S., Bhandari, A., Corominas, R., *et al*. (2011). Duplications of the neuropeptide receptor gene VIPR2 confer significant risk for schizophrenia. *Nature* 471, 499–503.

Vaiceliunaite, A., Erisken, S., Franzen, F., Katzner, S., and Busse, L. (2013). Spatial integration in mouse primary visual cortex. *J. Neurophysiol.* 110, 964–972.

Vergaelen, E., Claes, S., Kempke, S., and Swillen, A. (2017). High prevalence of fatigue in adults with a 22q11.2 deletion syndrome. *Am. J. Med. Genet. A* 173, 858–867.

Walz, K., Caratini-Rivera, S., Bi, W., Fonseca, P., Mansouri, D.L., Lynch, J., Vogel, H., Noebels, J.L., Bradley, A., and Lupski, J.R. (2003). Modeling del(17)(p11.2p11.2) and dup(17)(p11.2p11.2) contiguous gene syndromes by chromosome engineering in mice:

Phenotypic consequences of gene dosage imbalance. *Mol. Cell. Biol.* 23, 3646–3655.

Wang, H., Yang, H., Shivalila, C.S., Dawlaty, M.M., Cheng, A.W., Zhang, F., and Jaenisch, R. (2013). One-step generation of mice carrying mutations in multiple genes by CRISPR/Cas-mediated genome engineering. *Cell* 153, 910–918.

Wang, T., Wei, J.J., Sabatini, D.M., and Lander, E.S. (2014). Genetic screens in human cells using the CRISPR-Cas9 system. *Science* 343, 80–84.

Wapner, R.J., Martin, C.L., Levy, B., Ballif, B.C., Eng, C.M., Zachary, J.M., Savage, M., Platt, L.D., Saltzman, D., Grobman, W.A., *et al*. (2012). Chromosomal microarray versus karyotyping for prenatal diagnosis. *N. Engl. J. Med.* 367, 2175–2184.

Williams, H.J., Norton, N., Dwyer, S., Moskvina, V., Nikolov, I., Carroll, L., Georgieva, L., Williams, N.M., Morris, D.W., Quinn, E.M., *et al*. (2011). Fine mapping of ZNF804A and genome-wide significant evidence for its involvement in schizophrenia and bipolar disorder. *Mol. Psychiatry* 16, 429–441.

Wong, L.M., Riggins, T., Harvey, D., Cabaral, M. & Simon, T.J. (2014). Children with chromosome 22q11.2 deletion syndrome exhibit impaired spatial working Memory. *Am. J. Intellect. Dev. Disabil.* 119, 115–132.

Yeap, S., Kelly, S.P., Sehatpour, P., Magno, E., Javitt, D.C., Garavan, H., Thakore, J.H., and Foxe, J.J. (2006). Early visual sensory deficits as endophenotypes for schizophrenia: high-density electrical mapping in clinically unaffected first-degree relatives. *Arch. Gen. Psychiatry* 63, 1180–1188.

Yee, B.K., Chang, T., Pietropaolo, S., and Feldon, J. (2005). The expression of prepulse inhibition of the acoustic startle reflex as a function of three pulse stimulus intensities, three prepulse stimulus intensities, and three levels of startle responsiveness in C57BL6/J mice. *Behav. Brain Res. 163*, 265–276.

Young, J.W., Wallace, C.K., Geyer, M.A., and Risbrough, V.B. (2010). Age-associated improvements in cross-modal prepulse inhibition in mice. *Behav. Neurosci.* 124, 133–140.

Figures

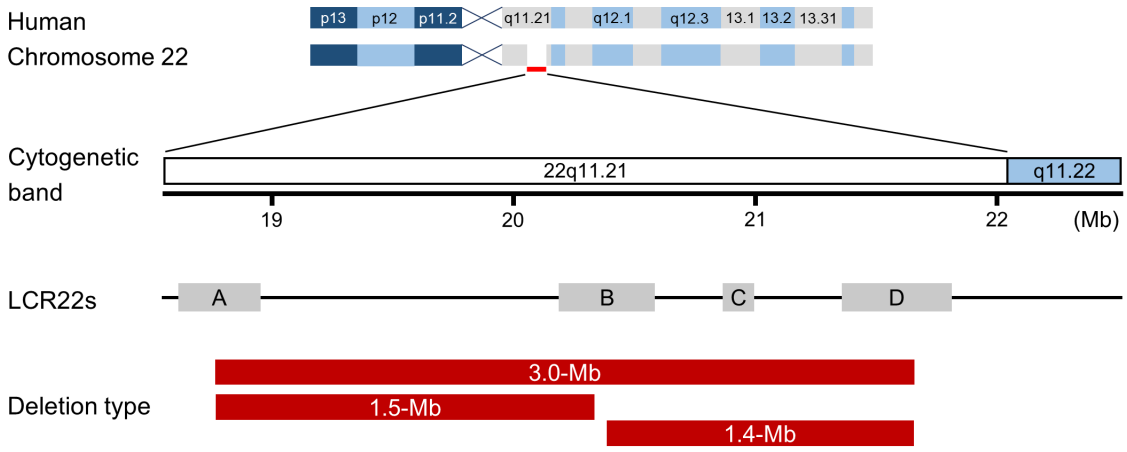

Figure 1. Schematic overview of the human chromosome 22q11.2 region.

Schematic illustration of human chromosome 22 and cytogenetic band of 22q11.21 region is shown at the top. Gray boxes indicate the low copy repeat A to D (LCR22A-D) that are the cause of deletion. Red horizontal bars indicate the deletion regions observed in patients.

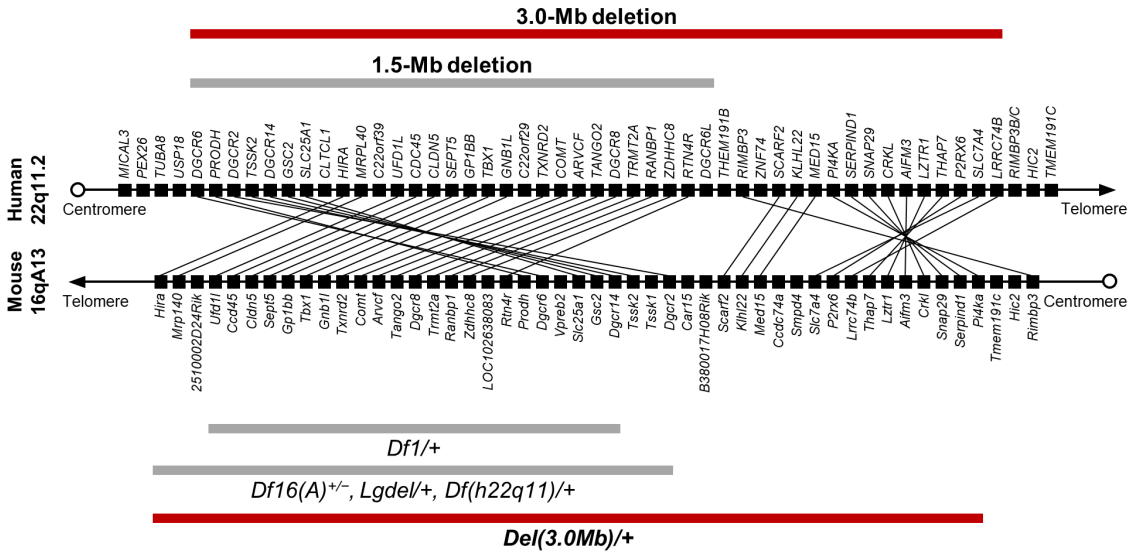

Figure 2. The human chromosome 22q11.2 region and the syntenic region of mouse chromosome 16qA13.

Each black box represents one gene. Red horizontal bars indicate the hemizygous genomic deletion most frequently (~90%) found in human 22q11.2DS (upper) and syntenic genomic deleted region of *Del(3.0Mb)/+* mice generated in this study (lower). Gray horizontal bars indicate the 1.5-Mb region less frequently (~7%) affected in 22q11.2DS (upper) and syntenic genomic region of previous mouse models (lower; *Df1/+*, *Df(16)A*$^{+/-}$, *Lgdel/+* and *Df(h22q11)/+*).

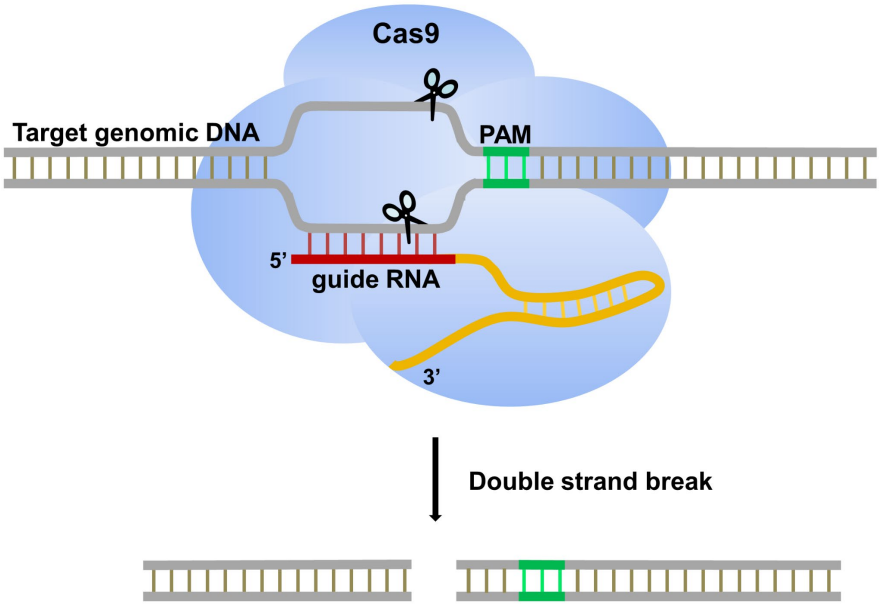

Figure 3. Mechanisms of CRISPR/Cas9-induced double-strand breaks in target genomic DNA.

Double strand break is induced by Cas9 endonuclease forming the complex with a guide RNA that is complementary to a 20-nucleotide target sequence. As Cas9 nuclease recognizes the target sequence, protospacer adjacent motif (PAM) that is a short specific sequence immediately following the guide RNA sequence on target DNA is required. Double strand break mediated by Cas9 occurs in 3 nt downstream of the PAM.

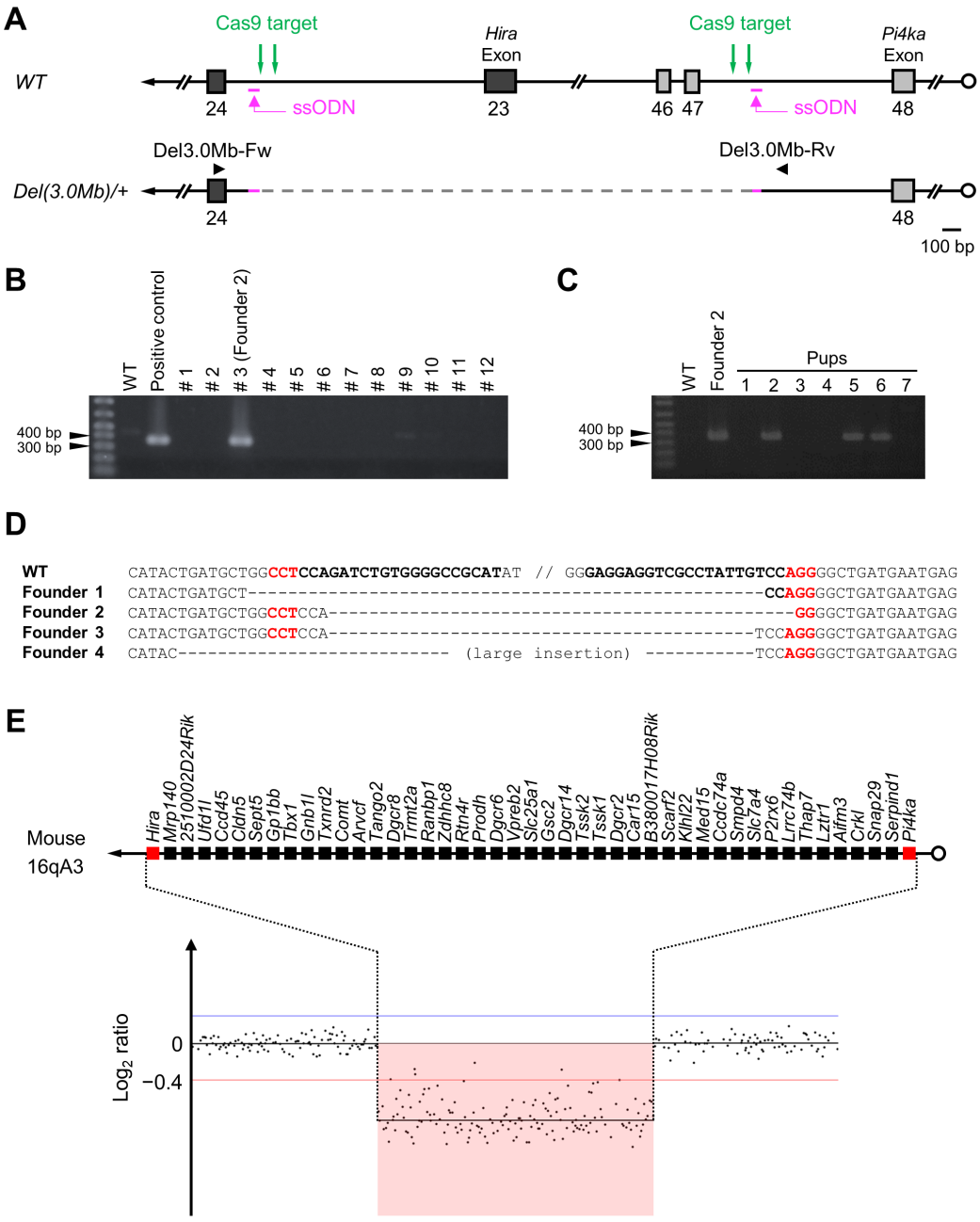

Figure 4. Generation and establishment of *Del(3.0Mb)/+* mice.

(A) Schematic illustration of WT and *Del(3.0Mb)/+* alleles. Green arrows, CRISPR/Cas9 target sites in *Hira* intron 23 and *Pi4ka* intron 47; pink bars, bridging single-stranded oligodeoxyribonucleotides (ssODNs); black squares, *Hira* exons; gray squares, *Pi4ka* exons; black arrowheads, PCR primers; dashed line, deleted region in the *Del(3.0Mb)/+* allele. (B) A representative result of genotyping PCR analysis of *Del(3.0Mb)/+* founder candidates. (C) Genotyping analysis of N1 offspring of *Del(3.0Mb)/+* founder × WT crossing. (D) The nucleotide sequence analysis of a PCR-amplified fragment around the deletion junction in *Del(3.0Mb)/+* founder

candidates. sgRNA sequences are indicated in bold and PAM sites in red. (E) Array CGH profile of chromosome 16qA13 from N1 *Del(3.0Mb)/+* mouse showing the decrease in copy number of targeting region (pink). Array CGH data are shown in a magnified view. Each black box represents one gene in the deleted region. Red boxes are CRISPR/Cas9 target genes (*Hira* and *Pi4ka*).

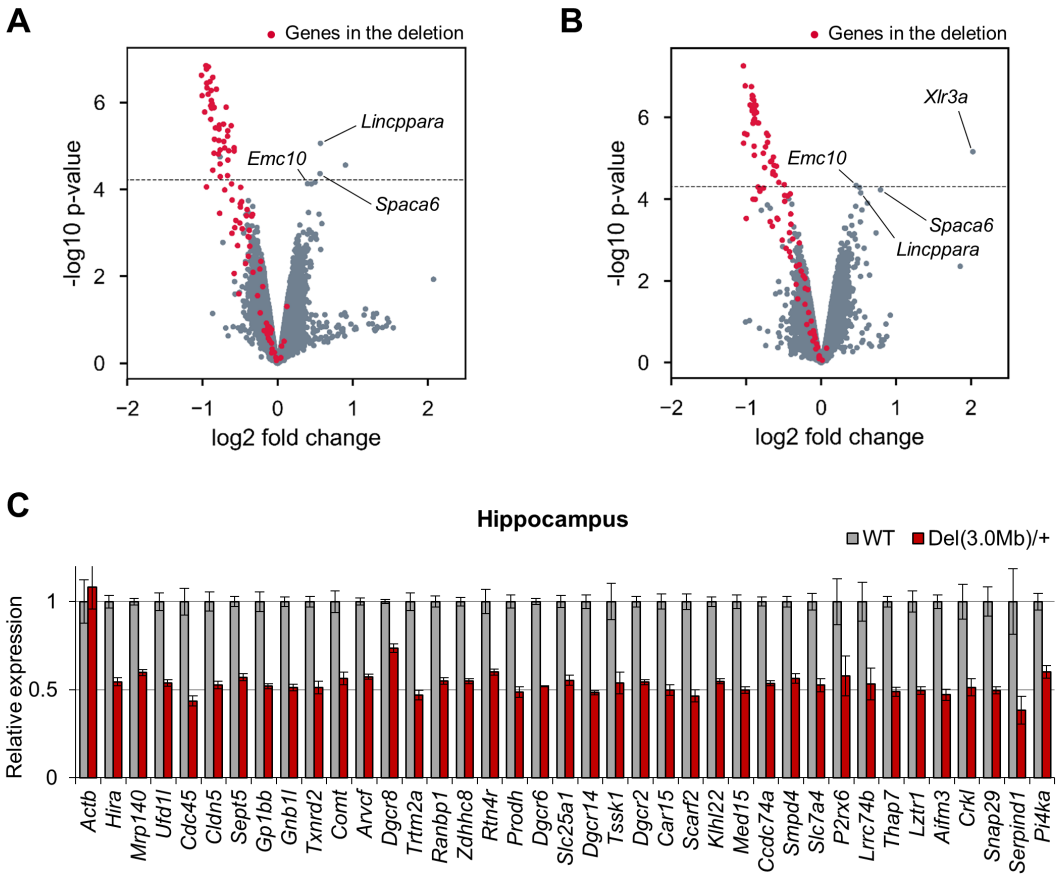

Figure 5. mRNA expression in the hippocampus and frontal cortex of *Del(3.0Mb)/+* mice.

(A) Volcano plot of the mRNA microarray analysis data of the hippocampus. The x-axis shows $\log_2$ of the fold change (*Del(3.0Mb)/+* vs. WT). The genes in the deleted region are depicted in red. The horizontal dashed line indicates the *p*-value of FDR = 0.05. miRNA host genes (*Lincppara* and *Spaca6*) and miR-185 target gene *Emc10* were upregulated in *Del(3.0Mb)/+* hippocampus. (B) Volcano plot of the mRNA microarray analysis data of the frontal cortex. The x-axis shows $\log_2$ of the fold change (*Del(3.0Mb)/+* vs. WT). The genes in the deleted region are depicted in red. The horizontal dashed line indicates the *p*-value of FDR = 0.05. (C) Quantitative RT-PCR analysis of mRNA from the hippocampus of WT (n = 5) and *Del(3.0Mb)/+* (n = 5) mice. The expression of all the genes in deleted region were significantly decreased in the hippocampus of *Del(3.0Mb)/+* mice ($p < 0.05$, two-tailed Welch's *t*-test). *Actb* gene was used as a control.

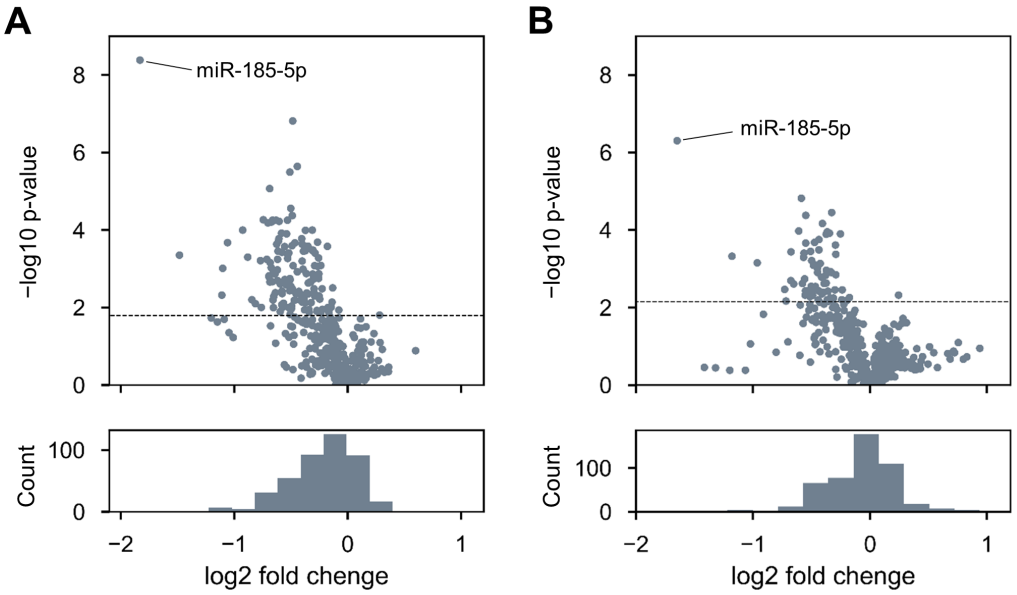

Figure 6. miRNA expression in the hippocampus and frontal cortex of *Del(3.0Mb)/+* mice.

(A) The microarray analysis of miRNA expression in the hippocampus. Top: Volcano plot of the microarray analysis data. The horizontal dashed line indicates the *p*-value of FDR = 0.05. Bottom: Histogram shows the distribution of the probesets across the fold change. (B) The microarray analysis of miRNA expression in the frontal cortex. Top: Volcano plot of the microarray analysis data. The horizontal dashed line indicates the *p*-value of FDR = 0.05. Bottom: Histogram shows the distribution of the probesets across the fold change.

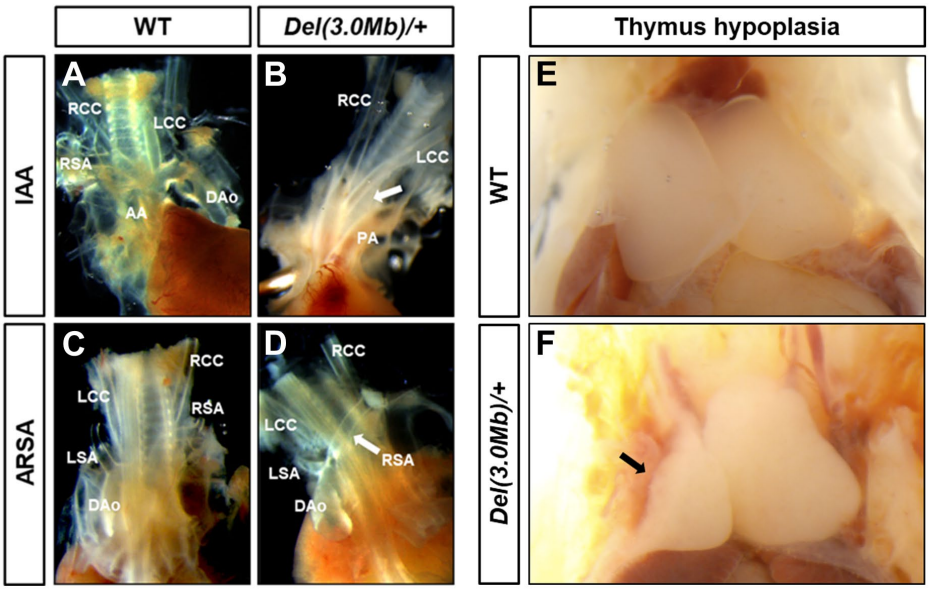

Figure 7. Cardiovascular and thymic defects in *Del(3.0Mb)/+* E18.5 embryos.

(A) Normal anatomy in a WT embryo. Observation of the heart from the ventral side. (B) Interrupted aortic arch (IAA) in a *Del(3.0Mb)/+* embryo. A white arrow shows the point of the anomaly. (C) Normal anatomy in a WT embryo. Observation of the heart from the dorsal side. (D) Aberrant right subclavian artery (ARSA) from the descending aorta in a *Del(3.0Mb)/+* embryo. A white arrow shows the abnormal blood vessel. AA, aortic arch; DAo, descending aorta; LCC, left common carotid artery; LSA, left subclavian artery; RCC, right common carotid artery; RSA, right subclavian artery. (E, F) Representative thymi from a WT control embryo (E) and a *Del(3.0Mb)/+* embryo (F). A black arrow shows thymic hypoplasia in a *Del(3.0Mb)/+* embryo.

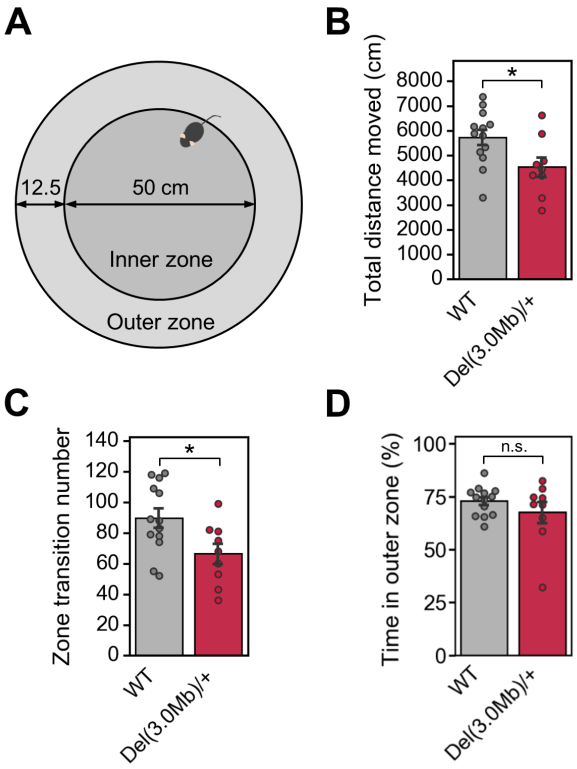

Figure 8. Assessment of general locomotor activity by open field test in *Del(3.0Mb)/+* mice.

(A) Schematic illustration of open field apparatus. (B) Total distance moved during the 10-min test period. (C) The number of transitions between the outer and inner zones. (D) Percentage of time spent in the outer zone. Data are expressed as the mean ± SEM (WT, n = 13; *Del(3.0Mb)/+*, n = 9). n.s.; not significant, **p* < 0.05 by two-tailed Welch's *t*-test.

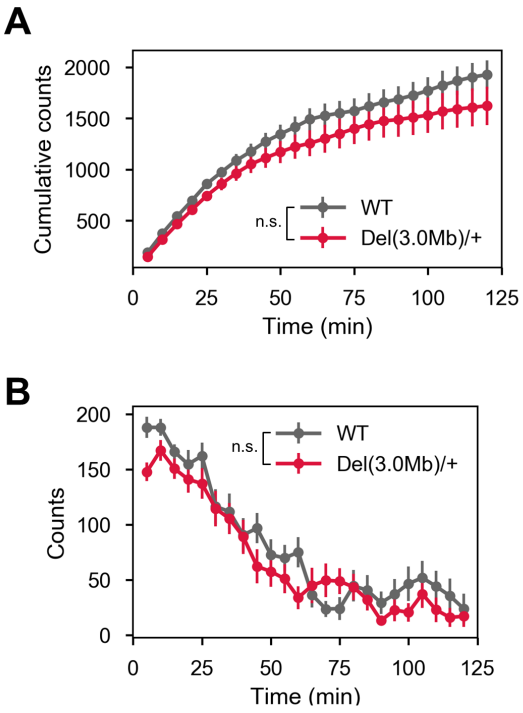

Figure 9. Assessment of long-term locomotor activity in *Del(3.0Mb)/+* mice.

(A) The cumulative count curves of the number of moving actions in 120 min. (B) The counts averaged in every 5 min. Data are expressed as the mean ± SEM (WT, n = 15; *Del(3.0Mb)/+*, n = 15). n.s.; not significant. Two-tailed Welch's *t*-test (A; at 120 min) or two-way ANOVA (B) were conducted to determine significant difference.

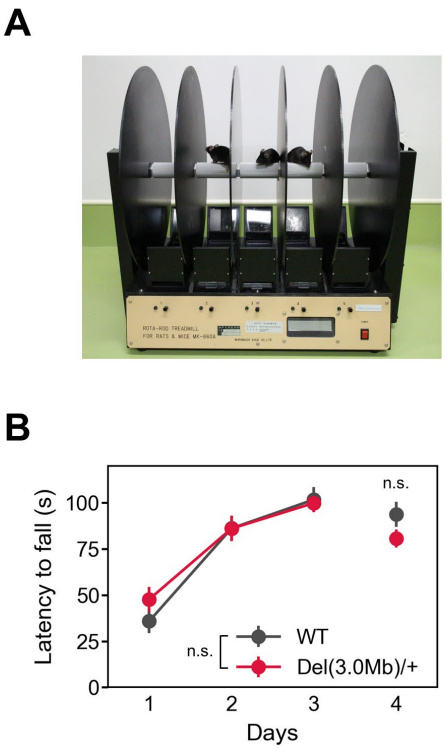

Figure 10. Evaluation of motor functions of *Del(3.0Mb)/+* mice by rotarod test.

(A) The rotarod apparatus. (B) Latency to fall off rotarod. Data are expressed as the mean ± SEM (WT, n = 15; *Del(3.0Mb)/+*, n = 15). n.s.; not significant. Two-way ANOVA (Day 1–3) or two-tailed Welch's *t*-test (Day 4) were conducted to determine significant difference.

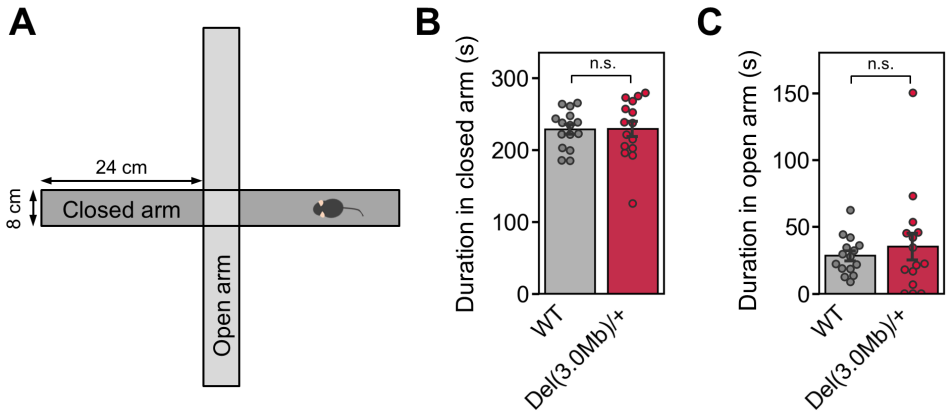

Figure 11. Evaluation of anxiety-like behavior of *Del(3.0Mb)/+* mice by elevated plus-maze test.

(A) Schematic illustration of elevated plus-maze apparatus. The apparatus was elevated to a height of 50 cm above floor level. (B) Time spent in closed arm. (C) Time spent in open arm. Data are expressed as the mean ± SEM (WT, n = 15; *Del(3.0Mb)/+*, n = 15). n.s.; not significant. Two-tailed Welch's *t*-test was conducted to determine significant difference.

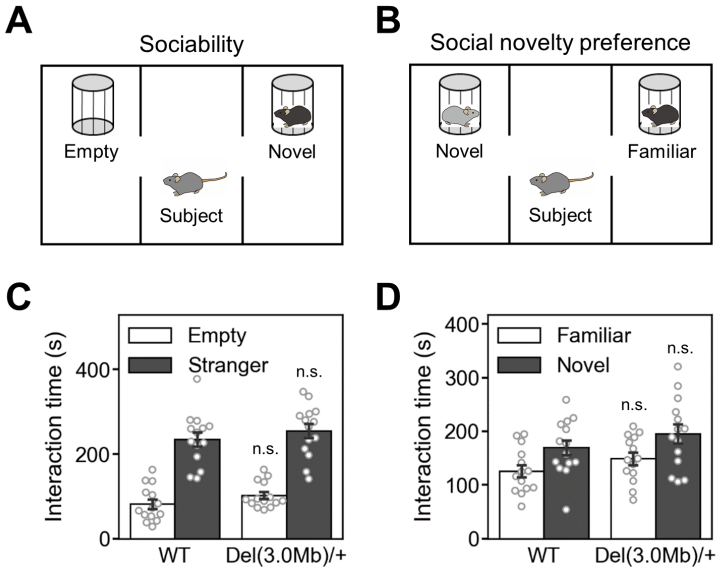

Figure 12. Assessment of social behavior of *Del(3.0Mb)/+* by three-chamber social interaction test.

(A) Schematic diagram of the sociability phase in the three-chamber test. (B) Schematic diagram of social novelty preference phase in the three-chamber test. (C) Interaction time of the sociability test. (D) Interaction time of the social novelty test. Data are expressed as the mean ± SEM (WT, n = 15; *Del(3.0Mb)/+*, n = 15). n.s.; not significant. Two-tailed Welch's *t*-test was conducted to determine significant difference.

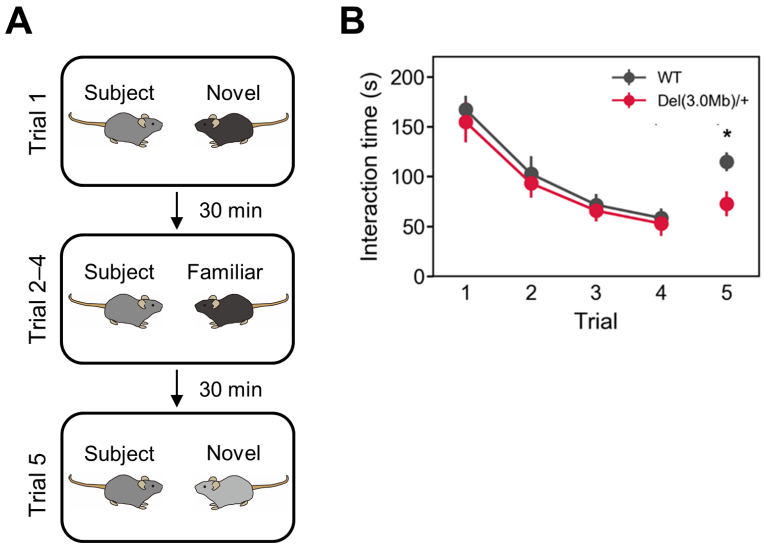

Figure 13. Performance of five-trial direct social interaction test in *Del(3.0Mb)/+* mice.

(A) Schematic diagram of five-trial direct social interaction test. A subject mouse was habituated to the same intruder of a juvenile mouse (trial 1–4) and dishabituated toward a novel mouse (trial 5). Each 5-min trial was separated by a 30-min interval. (B) Time length spent interacting with the intruder was evaluated. Data are expressed as the mean ± SEM (WT, n = 13; *Del(3.0Mb)/+*, n = 9). **p* < 0.05. n.s.; not significant. Two-way ANOVA (trial 1–4) or two-tailed Welch's *t*-test (trial 5) were conducted to determine significant difference.

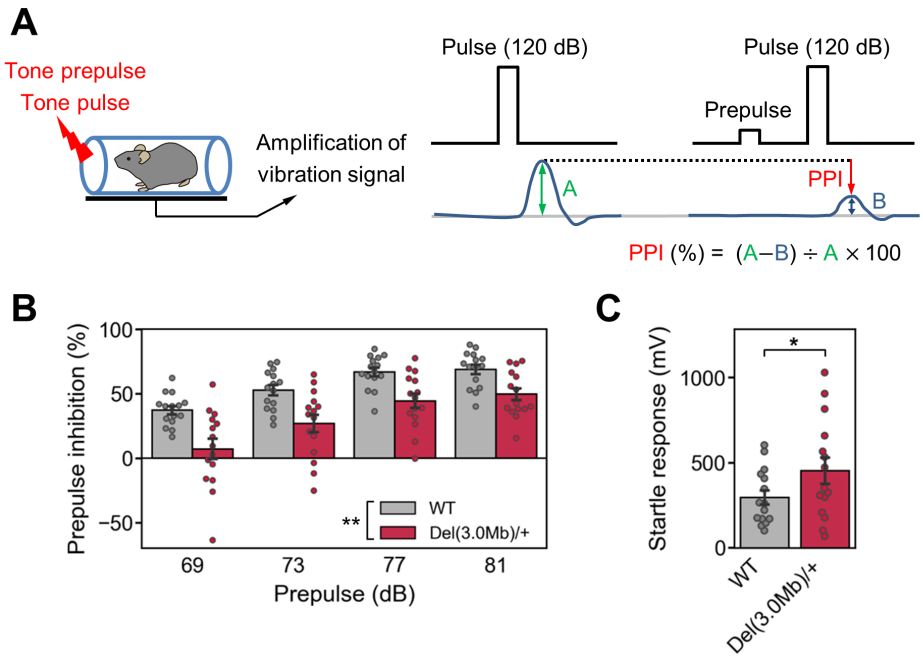

Figure 14. Assessment of sensorimotor gating in *Del(3.0Mb)/+* mice by auditory PPI.

(A) Schematic illustration of auditory PPI procedure. A subject mouse is placed in a Plexiglas cylinder and exposed to tone stimuli. PPI is a neurological phenomenon in which a weak acoustic stimulus (prepulse) inhibits a reflexive startle response induced by the subsequent intense startling stimulus (pulse). PPI (%) was calculated with the formula shown in the figure. (B) Percentage of auditory PPI, which was measured at four different prepulse levels (69, 73, 77 and 81dB). (C) Measurements of acoustic startle responses to the 120-dB startle stimulus. Data are expressed as the mean ± SEM (WT, n = 15; *Del(3.0Mb)/+*, n = 15). *$p < 0.05$, **$p < 0.01$. Two-way ANOVA (B) or two-tailed Welch's *t*-test (C) were conducted to determine significant difference.

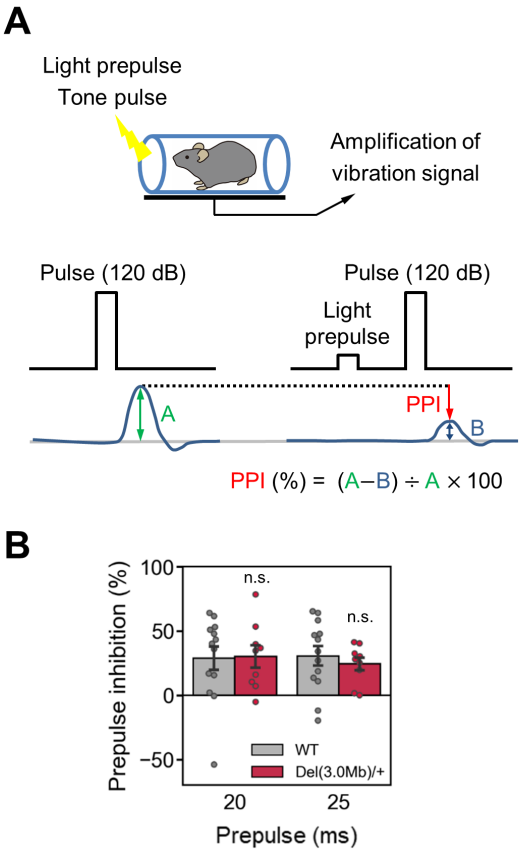

Figure 15. Assessment of sensorimotor gating in *Del(3.0Mb)/+* mice by visual PPI.

(A) Schematic illustration of visual PPI procedure. A subject mouse is exposed to light stimuli (prepulse) and tone stimuli (pulse). PPI (%) was calculated with the formula shown in the figure. (B) Percentage of visual PPI, which was measured at two conditions of light prepulse duration (20 or 25 ms). Data are expressed as the mean ± SEM (WT, n = 13; *Del(3.0Mb)/+*, n = 9). n.s.; not significant. Two-way ANOVA were conducted to determine significant difference.

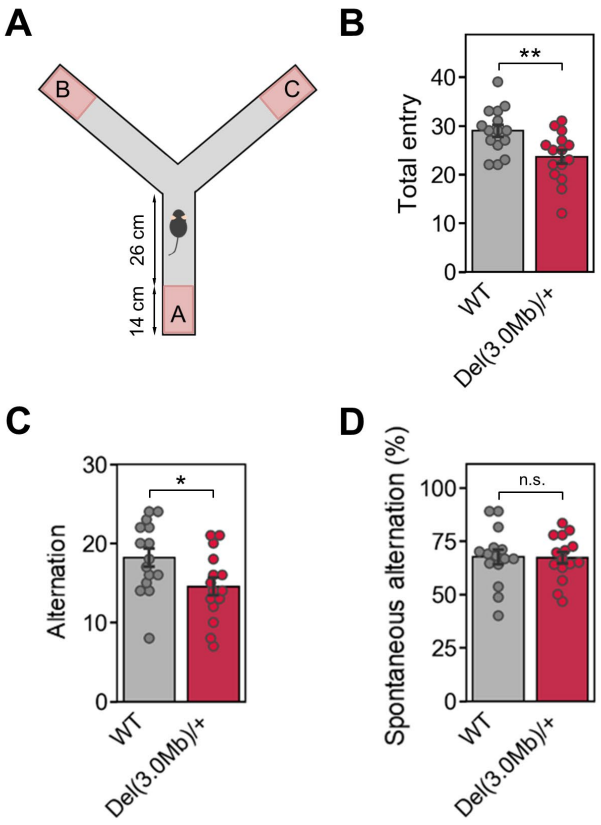

Figure 16. Evaluation of spatial working memory of *Del(3.0Mb)/+* mice by Y-maze test.

(A) Schematic diagram of Y-maze apparatus. Red area indicates criteria for entering arms. (B) The total number of arm entries. (C) The number of spontaneous alternations. (D) Percentage of spontaneous alternations. Data are expressed as the mean ± SEM (WT, n = 15; *Del(3.0Mb)/+*, n = 15). n.s.; not significant, *$p < 0.05$, **$p < 0.01$ by two-tailed Welch's *t*-test.

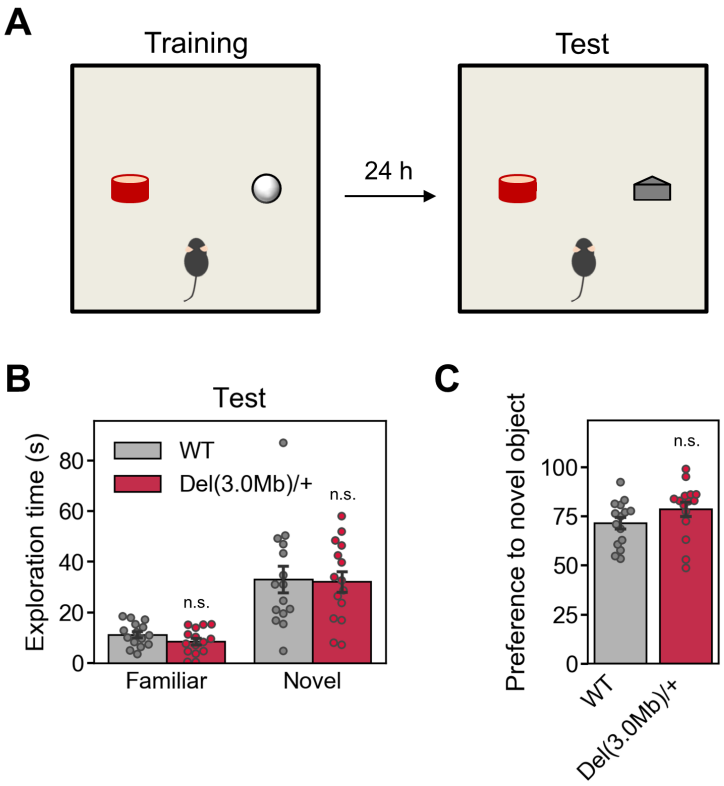

Figure 17. Measurement of recognition memory in *Del(3.0Mb)/+* mice by novel object recognition test. (A) Schematic illustration of novel object recognition test. (B) The data of exploration time to familiar and novel object in test phase. (C) Percentage of exploratory preference to each of objects. Data are expressed as the mean ± SEM (WT, n = 15; *Del(3.0Mb)/+*, n = 15). n.s.; not significant. Two-tailed Welch's *t*-test was conducted to determine significant difference.

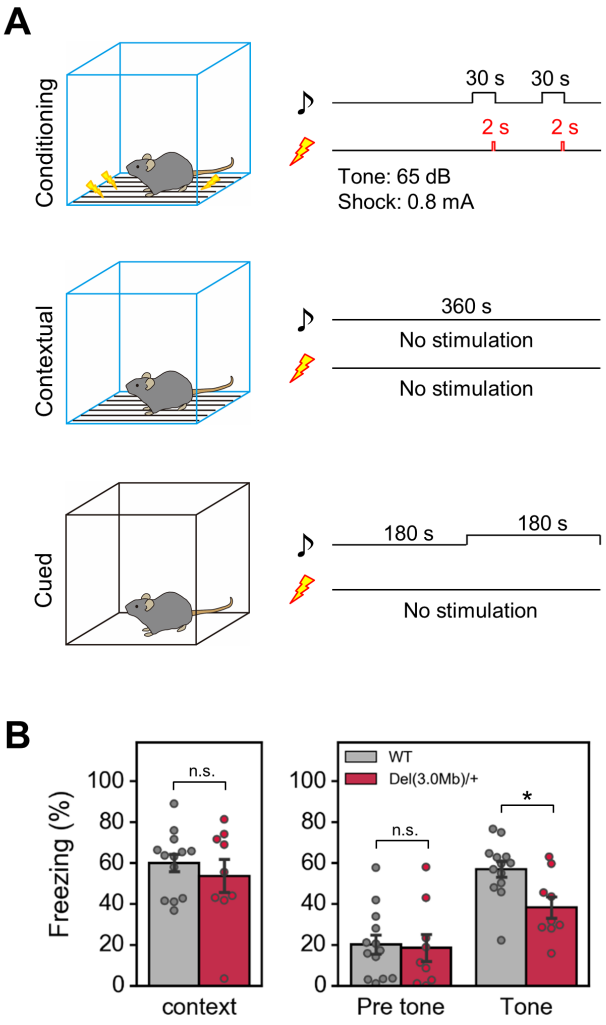

Figure 18. Assessment of associative learning and memory in *Del(3.0Mb)/+* mice by fear-conditioning test.

(A) Schematic diagram of the outline of behavioral paradigm and stimulation conditions. (B) The data of freezing response in each of test phases. Shown on the left panel is a context-dependent freezing response (%) towards the tone and foot-shock paring (conditioning) measured 24 h after the initial exposure. Shown on the right panel is a cue-dependent freezing response (%) measured 48 h after the conditioning. Data are expressed as the mean ± SEM (WT, n = 13; *Del(3.0Mb)/+*, n = 9). n.s.; not significant, $*p < 0.05$ by two-tailed Welch's *t*-test.

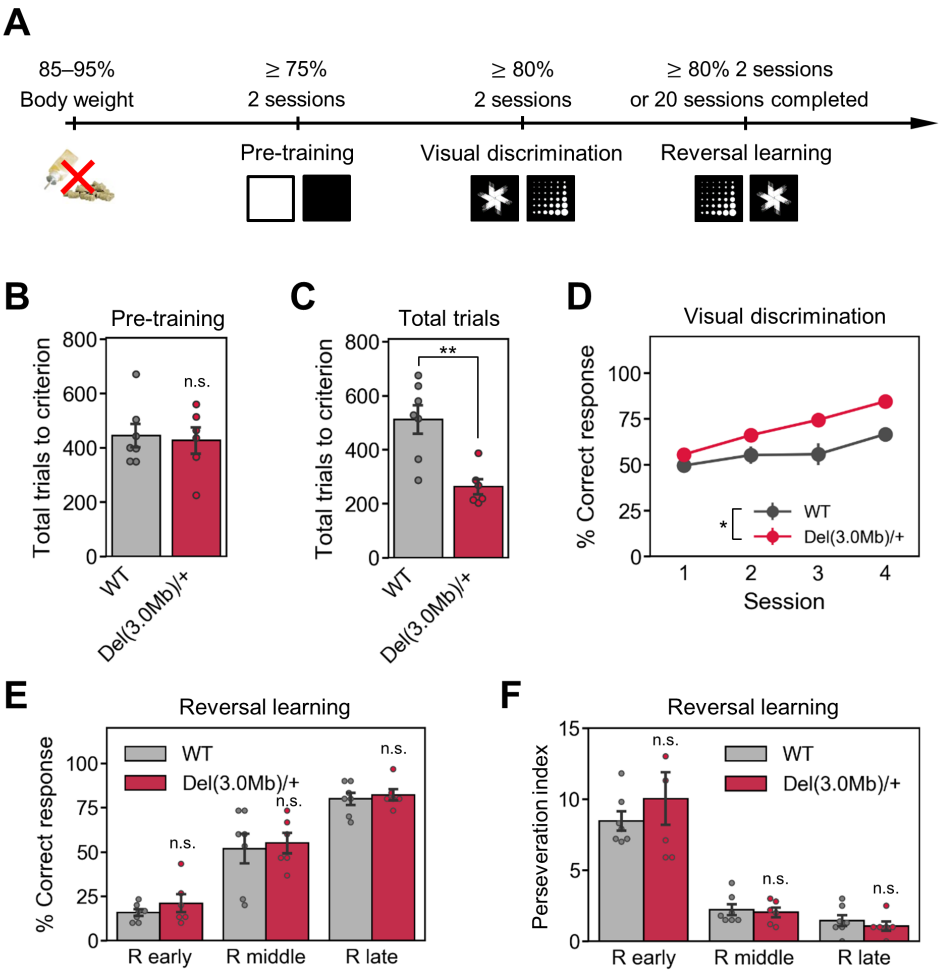

Figure 19. Performance of *Del(3.0Mb)/+* mice in visual discrimination (VD) and reversal learning.

(A) Experimental schedule for VD task and reversal learning tasks. (B) A total number of trials to reach the criterion in the pre-training task. (C) A total number of trials to reach the criterion in VD task. (D) Acquisition of the first 4 sessions in VD learning. (E) Percentage of correct responses in reversal learning task. (F) Perseveration index on the early, middle and late stages of reversal learning. R early, first reversal learning session. R middle, session midway through reversal session. R late, final reversal session. Data are expressed as the mean ± SEM (WT, n = 7; *Del(3.0Mb)/+*, n = 6). n.s.; not significant, *$p < 0.05$, **$p < 0.01$. Two-tailed Welch's *t*-test (B, C, E and F) of two-way ANOVA (D) were conducted to determine significant difference.

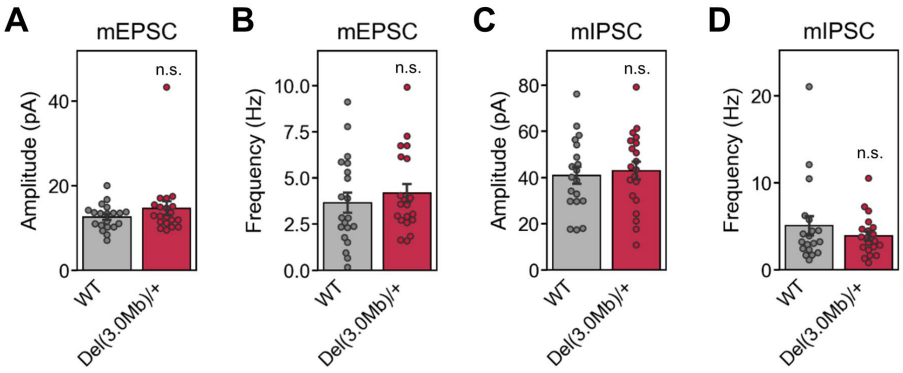

Figure 20. Basal synaptic transmission in the mPFC of *Del(3.0Mb)/+* mice.

Layer 2/3 pyramidal neurons in acute mPFC slices from 2-week-old *Del(3.0Mb)/+* and WT littermates were whole-cell patch clamped and miniature excitatory postsynaptic currents (mEPSCs) and miniature inhibitory postsynaptic currents (mIPSCs) were recorded. (A) The amplitude of mEPSC. (B) The frequency of mEPSC. (C) The amplitude of mIPSC. (D) The frequency of mIPSC. Data are expressed as the mean ± SEM (n = 19–20 cells from WT control mice and n = 20 cells from *Del(3.0Mb)/+* mice). Two-tailed Welch's *t*-test was conducted to determine significant difference. n.s.; not significant.

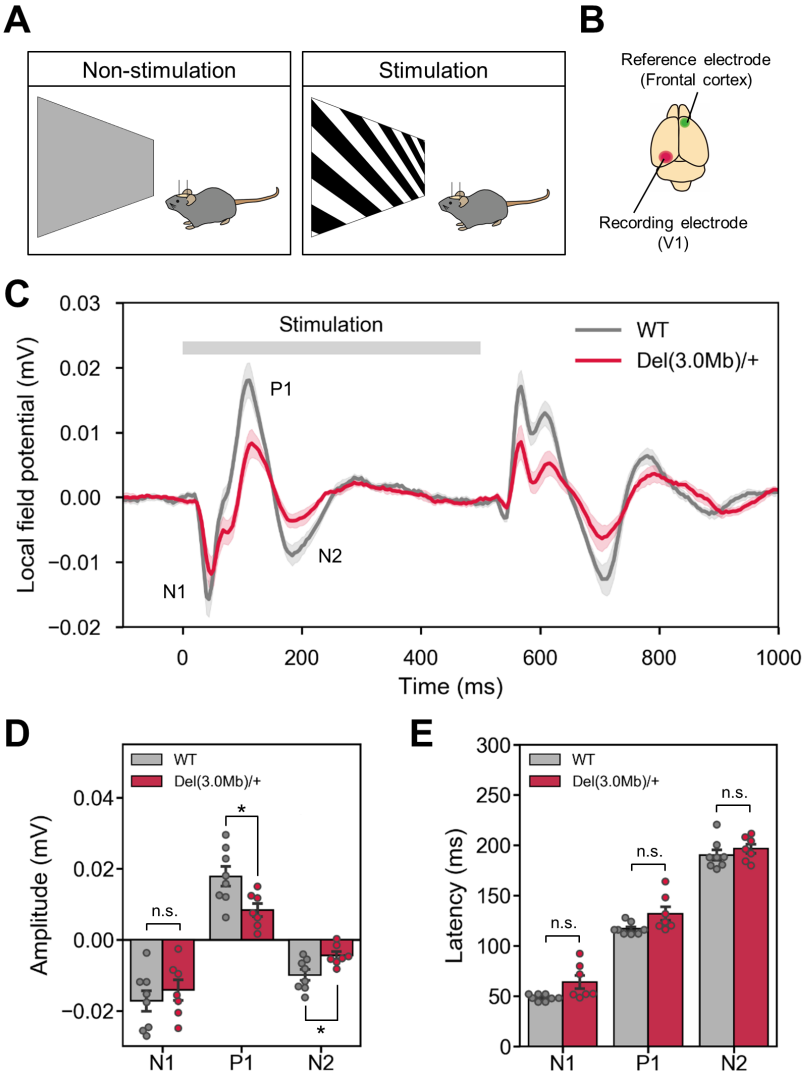

Figure 21. Measurements of the visual evoked potential in *Del(3.0Mb)/+* mice.

(A) Schematic diagram of the experimental set-up for measuring the visual evoked potential. (B) A recording electrode and a reference electrode were implanted into the primary visual cortex (V1) and the frontal cortex, respectively. (C) The wave forms of the grand mean of time-averaged local field potential. (D) The mean amplitudes of negative and positive potentials (N1, P1 and N2 indicated in C). (E) The mean latency of negative and positive potential peaks (N1, P1 and N2). All data are expressed as the mean ± SEM (WT, n = 8; *Del(3.0Mb)/+*, n = 7). n.s.; not significant, $*p < 0.05$ by two-tailed Welch's *t*-test.

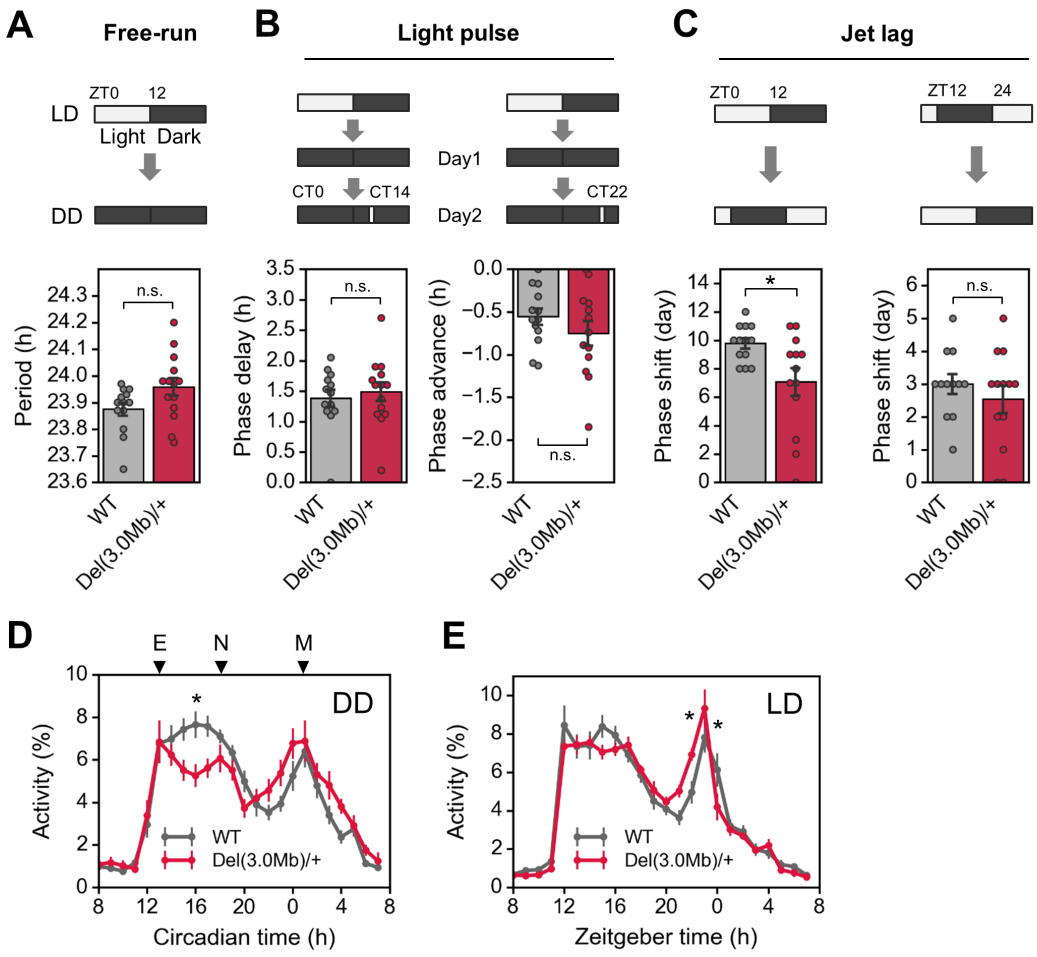

Figure 22. Measurement of circadian behavioral rhythm of *Del(3.0Mb)/+* mice.

Circadian activity and its re-entrainment by ambient light. (A) The upper panel shows a schematic diagram of light-dark cycle. Spontaneous locomotor activities of WT mice (n = 13) and *Del(3.0Mb)/+* mice (n = 14) were measured by an infrared thermal sensor. Free-running period of circadian behavioral rhythm was calculated by a χ^2 periodogram (lower panel). (B) Phase shifting responses to a 30-min light pulse at CT14 (WT, n = 13; *Del(3.0Mb)/+*, n = 14) and CT22 (WT, n = 13; *Del(3.0Mb)/+*, n = 13). (C) Responses to rescheduled light-dark cycles with 8-h advance (WT, n = 13; *Del(3.0Mb)/+*, n = 13) and 8-h delay (WT, n = 12; *Del(3.0Mb)/+*, n = 13). The number of days required to adapt to a new light-dark cycle was counted. (D, E) Activity profile in DD (D) and LD (E) (WT, n = 13; *Del(3.0Mb)/+*, n = 14). Data from day 7 through 17 in constant dark condition were used for the calculation of the circadian periods and the activity profiles. n.s.; not significant, *$p < 0.05$. Two-tailed Welch's *t*-test (A, B and C) or two-way ANOVA (D and E) were conducted to determine significant difference.

Tables

Table 1. Comparison of 22q11.2DS-related phenotypes in mouse models.

Mouse models	Deletion	Number of deleted genes	Method	ES or zygote cell background	Additional background
Del(3.0Mb)/+	*Hira-Pi4ka*	46	CRISPR/Cas9	C57BL/6N	C57BL/6N, 3-5 backcrosses
Df(h22q11)/+	*Hira-Dgcr2*	29	Cre/*loxP*	C57BL/6NTac	C57BL/6N
Df(h22q11)/+	*Hira-Dgcr2*	29	Cre/*loxP*	C57BL/6NTac	C57BL/6N
Df(16)A $^{+/-}$	*Hira-Dgcr2*	29	Cre/*loxP*	129S7/SvEvBrd-*Hprt* $^{b-m2}$	C57BL/6J, 3 backcrosses
Df(16)A $^{+/-}$	*Hira-Dgcr2*	29	Cre/*loxP*	129S7/SvEvBrd-*Hprt* $^{b-m2}$	C57BL/6J, >10 backcrosses
Df(16)A $^{+/-}$	*Hira-Dgcr2*	29	Cre/*loxP*	129S7/SvEvBrd-*Hprt* $^{b-m2}$	C57BL/6J
Df(16)A $^{+/-}$	*Hira-Dgcr2*	29	Cre/*loxP*	129S7/SvEvBrd-*Hprt* $^{b-m2}$	C57BL/6J, >10 backcrosses
Lgdel/+	*Hira-Dgcr2*	29	Cre/*loxP*	129Sv, C57BL/6J, SJL	C57BL/6N, >25 backcrosses
Lgdel/+	*Hira-Dgcr2*	29	Cre/*loxP*	129Sv, C57BL/6J, SJL	C57BL/6J
Df1/+	*Dgcr14-Ufd1l*	23	Cre/*loxP*	129S7/SvEvBrd-*Hprt* $^{b-m2}$	129S5/SvEvBrd; C57BL/6$^{c-/c-}$, 4 or 5 backcrosses
Df1/+	*Dgcr14-Ufd1l*	23	Cre/*loxP*	129S7/SvEvBrd-*Hprt* $^{b-m2}$	129S5/SvEvBrd; C57BL/6$^{c-/c-}$, 5-6 backcrosses
Df1/+	*Dgcr14-Ufd1l*	23	Cre/*loxP*	129S7/SvEvBrd-*Hprt* $^{b-m2}$	C57BL/6J, >10 backcrosses
Df1/+	*Dgcr14-Ufd1l*	23	Cre/*loxP*	129S7/SvEvBrd-*Hprt* $^{b-m2}$	C57BL/6J, >12 backcrosses
Human (22q11.2DS)					
3.0-Mb deletion (~90%)	**DGCR6-LRRC74B***	**45**			
1.5-Mb deletion (~7%)	**DGCR6-DGCR6L***	**29**			

(*Table continued on next page*)

(*Continued*)

Mouse models	Open field		Y-maze	Elevated-plus maze	Novel object recognition	Locomotor activity	Social interaction		Prepulse inhibition	
	Total	Margin					Three-camber	Direct	Auditory	Visual
Del(3.0Mb)/+	↓	n.c.	n.c.	n.c.	n.c.	120 min: n.c.	n.c.	Recognition: ↓	↓	n.c.
Df(h22q11)/+	N/A	N/A	n.c.	N/A	n.c.	N/A	N/A	N/A	N/A	N/A
Df(h22q11)/+	N/A	N/A	N/A	n.c.	N/A	N/A	N/A	N/A	↓	N/A
Df(16)A $^{+/-}$	↑	↑	N/A	N/A	N/A	N/A	N/A	N/A	↓	N/A
Df(16)A $^{+/-}$	N/A	N/A	N/A	N/A	n.c.	N/A	N/A	N/A	N/A	N/A
Df(16)A $^{+/-}$	N/A	N/A	N/A	N/A	N/A	N/A	N/A	Basal SI: n.c. Memory: ↓	N/A	N/A
Df(16)A $^{+/-}$	↑	↑	N/A	N/A	N/A	N/A	N/A	Basal SI: n.c. Memory: ↓	↓	N/A
Lgdel/+	N/A	N/A	N/A	N/A	N/A	N/A	N/A	N/A	N/A	N/A
Lgdel/+	↑	N/A	N/A	N/A	N/A	N/A	N/A	N/A	N/A	N/A
Df1/+	n.c.	N/A	N/A	N/A	N/A	N/A	N/A	N/A	↓	N/A
Df1/+	N/A	N/A	N/A	N/A	N/A	N/A	N/A	N/A	↓	N/A
Df1/+	N/A	N/A	N/A	N/A	N/A	N/A	N/A	N/A	N/A	N/A
Df1/+	N/A	N/A	N/A	N/A	N/A	N/A	N/A	N/A	↓	N/A
Human (22q11.2DS) 3.0-Mb deletion (~90%) 1.5-Mb deletion (~7%)	Hyperactivity (ADHD): ↑[a]	Anxiety: ↑[b]	Spatial working memory: ↓[c]	Anxiety: ↑[b]	Object recognition: ↓[d]	Hyperactivity (ADHD):↑[a]	Social interaction: ↓[e]		Auditory PPI: ↓[f]	N/A

(*Table continued on next page*)

(*Continued*)

Mouse models	Acoustic startle response	Rotarod	Fear-conditioning		Visual discrimination		Reversal learning		Reference
			Context	Cue	Acquisition	Accuracy	Acquisition	Accuracy	
Del(3.0Mb)/+	**120 dB: ↑**	**n.c.**	**n.c. (24 h)**	**↓(48 h)**	**↑**	**↑**	**n.c.**	**n.c.**	**Present study**
Df(h22q11)/+	**N/A**	**N/A**	**n.c. (24 h)**	**n.c. (48 h)**	**↑**	**↑**	**↑**	**↑**	**Nilsson et al., 2016**
Df(h22q11)/+	**100 dB: ↑**	**N/A**	**N/A**	**N/A**	**N/A**	**N/A**	**N/A**	**N/A**	**Didriksen et al., 2017**
Df(16)A $^{+/-}$	**N/A**	**N/A**	**↓ (24 h); n.c. (48 h)**	**↓ (48 h)**	**N/A**	**N/A**	**N/A**	**N/A**	**Stark et al., 2008**
Df(16)A $^{+/-}$	**N/A**	**N/A**	**↓ (24 h)**	**↓ (48 h)**	**N/A**	**N/A**	**N/A**	**N/A**	**Fenelon et al., 2013**
Df(16)A $^{+/-}$	**N/A**	**N/A**	**N/A**	**N/A**	**N/A**	**N/A**	**N/A**	**N/A**	**Piskorowski et al., 2016**
Df(16)A $^{+/-}$	**n.c.**	**N/A**	**↓ (24 h)**	**↓ (48 h)**	**N/A**	**N/A**	**N/A**	**N/A**	**Diamantopoulou et al., 2017**
Lgdel/+	**N/A**	**N/A**	**N/A**	**N/A**	**↓**	**N/A**	**↓**	**↓**	**Meechan et al., 2015**
Lgdel/+	**N/A**	**N/A**	**↓ (24 h)**	**N/A**	**N/A**	**N/A**	**N/A**	**N/A**	**Marissal et al., 2018**
Df1/+	**↑**	**n.c.**	**↓ (24 h); n.c. (1 h)**	**↓ (24 h)**	**N/A**	**N/A**	**N/A**	**N/A**	**Paylor et al., 2001**
Df1/+	**N/A**	**N/A**	**N/A**	**N/A**	**N/A**	**N/A**	**N/A**	**N/A**	**Paylor et al., 2006**
Df1/+	**N/A**	**N/A**	**N/A**	**↓ (24 h)**	**N/A**	**N/A**	**N/A**	**N/A**	**Eom et al., 2017**
Df1/+	**n.c.**	**↓**	**N/A**	**N/A**	**N/A**	**N/A**	**N/A**	**N/A**	**Sumitomo et al., 2018**
Human (22q11.2DS) 3.0-Mb deletion (~90%) 1.5-Mb deletion (~7%)	**n.c.**[g]	**Motor coordination: ↓**[h]	**Memory: ↓**[i]		**Visual perception: ↓**[d]		**Cognitive flexibility: ↓**[j]		**Detailed information of references are provided in footnote.**

↑, increase or improve behavior; ↓, decrease or impaired behavior; n.c., not changed; N/A, not applicable. Total, total distance moved in open field test; Margin, distance moved in margin zone; Basal SI, basal social interaction; PPI, prepulse inhibition. Parenthesis in the fear-conditioning column expresses the time that has elapsed from the conditioning phase. *Deletion length varies from individual patients. [a]Schneider et al., 2014; [b]Fung et al., 2010; [c]Wong et al., 2014; [d]McCabe et al., 2016; [e]Fine et al., 2005; [f]Sobin et al., 2005a; [g]Sobin et al., 2005b; [h]Cunningham et al., 2018; [i]Debbane et al., 2008; [j]Shapiro et al., 2014.

Table 2. sgRNA and single-stranded oligodeoxyribonucleotides (ssODN) sequences for generating *Del(3.0Mb)/+* mice.

sgRNA	sequences (5'–3')	ssODN 3.0-Mb bridge (5'–3')
Pi4ka sg1	CAGGACTGGGACTCGAGACGGGG	GCCAGAGCCTGATGCTCCCTTGC AGGAGCACGGCCACCTCCATACT GATGCTGGCCTCCATCCAGGGGC TGATGAATGAGTGAGGAACTATT CATGGTTCTCTAGGCCTCAAGTAG AAAG
Pi4ka sg2	ATGCGGCCCCACAGATCTGGAGG	
Hira sg1	GAGGAGGTCGCCTATTGTCCAGG	
Hira sg2	GGTAGAAGGAGTGGGCTAACAGG	

Table 3. Primer sequences for quantitative RT-PCR.

Gene	Forward	Reverse
Hprt	GGTTAAGCAGTACAGCCCCA	GTCTGGCCTGTATCCAACACT
Actb	CCTTCTTGGGTATGGAATCCTGT	TGGCATAGAGGTCTTTACGGATG
Pi4ka	GGCTGGGAACCAGACATCAA	CATCCATATAGGGGCGCACA
Serpind1	GCCATTGACCTGTTCAAGCA	GGGACGGTCGACAGTGAATC
Snap29	AACCTAGATGAGCTGTCCGTG	TGGTTGTCAGTCGGTCAAGG
Crkl	ACGTGCTAGATAACCGGCTG	TTTCAGCTGAGGCTGGGATG
Aifm3	CTTGCCTGGAGGAACAATCG	CATGGCAGTCCACAGATAGGG
Lztr1	GGCTTACTGCAAGCAAAACCT	GCAGCTTAGAGACCTTGGTGA
Thap7	CTGGTGGGAATCAGTGGGTA	TGTTCGACGCAACTTGGAGA
Lrrc74b	TGACCTGGCAGGAGAGATACT	CAGACCTCGCAGGTGATTCC
P2rx6	GAAGTTCGCGCTCATCCCTA	GGGGCTCTTGCCTCTTCATA
Slc7a4	CTGGTCGGACTTGTCGTGT	CTCCCGGACTGGTGATTGAC
Smpd4	CCGGAGCTACGAAATCACCA	TCTGGCCTGCAAATCTACGG
Ccdc74a	GAGATCGAGCACCTGAAGCG	GAGAGTTGGCGGACATCGTG
Med15	CACCTATCGTGTCGCCAGTG	ACCTTGCAGCACATTGGGTA
Klhl22	CCCCACTCAAGAAGGAGGTAT	TATGCCACGTGTTGCTTCCT
Scarf2	GAAGGCGCCTCAACGTTTTT	ATGGGCCACTACGACTTTGG
Car15	CATGCGCAGGTAGTCCAGTT	GGGGCGGAAATTACTCGTGA
Dgcr2	TTCCATTTCCACGACCCTCC	CTCAAAGGCATCGTCATCTGC
Tssk1	CGGTCTGAGTCAAAACCCCA	GGCTGCAAGAGGCTCACTAA
Dgcr14	ACTTGGCCAGTCTTACTCCCA	GAGGTGGGAAGATCGTGCTG
Slc25a1	TGCAGCCAGTGTCTTTGGAA	GTAGAATGCCTTTGGCCCCT
Dgcr6	CGAACACCGAGTGCTCAGAC	ATCCGATGTTCCATGGCCT
Prodh	TTTATGCCCAAGGCGGGATT	TTGGGGTACAGGAAGTCCCA
Rtn4r	GAGCTTCCAGTCATGCCGAA	GGTCCACGACATGAAGCTGT
Zdhhc8	AGAAACCTCTGGACCTGGGA	TGATAGGGCACTCTCAGCAC
Ranbp1	CTTCCTAAATGCTGAGAATGCAC	CCTCCCTCACTGAAAGGGC
Trmt2a	TAAGGTGATTCTGGCCATCCG	CCTGCAGAGGTCCACAAAGTT
Dgcr8	GCGCGGGTGGTGTAAGAATAA	TGCTGCTCTCACGACCATAC
Arvcf	ACGAAGTCACGCTTCCAGTC	TTGACTTCTCCCCATCAAGGC
Comt	ATTGTGGCTACTCAGCCGTG	CCCGATGAGGATGGAAACTTTG
Txnrd2	GGATCAAGTGTGGGGCTTCA	GCAACCAGTCACAGTAGGCT

(Table continued on next page)

(Continued)

Gene	Forward	Reverse
Gnb1l	TCCCTGCAGGTGAAGAAGACT	AACACACGGATGCGATGGTC
Gp1bb	AGTGATGGAACAGCCCAGTC	TTTGGCAAAGTCGGGTGGTA
Sept5	AACATGCTCATCCGCACTCA	CTGGGTGAGTTTGCTGGTCA
Cldn5	GTTAAGGCACGGGTAGCACT	TACTTCTGTGACACCGGCAC
Cdc45	GAGGGCACTCCAGATGTCAC	GCATCGTCGATTCTTTGTCGAG
Ufd1l	TTGAAGAGGATGAAGCTGGAGG	CAGTAACTGTAAGCCAGGTGC
Mrpl40	GCAGCAAAGGATCGCTTGAA	CTCCTGAGGTCGCTGTCTTG
Hira	CCTCCAACTCTGGAAGGCAAG	AGGAGGAGCCAGTGACGATA

Table 4. Statistical analysis related to Figure 8–22.

Figure 8B	Two-tailed Welch's *t*-test. $t_{16.68} = 2.393$. $^{*}p = 0.0288$. WT: n = 13, *Del(3.0Mb)/+*: n = 9.
Figure 8C	Two-tailed Welch's *t*-test. $t_{18.56} = 2.531$. $^{*}p = 0.0206$. WT: n = 13, *Del(3.0Mb)/+*: n = 9.
Figure 8D	Two-tailed Welch's *t*-test. $t_{10.36} = 0.996$. $p = 0.3420$. WT: n = 13, *Del(3.0Mb)/+*: n = 9.
Figure 9A	Cumulative counts at 120 min: Two-tailed Welch's *t*-test. $t_{25.9} = 1.295$. $p = 0.2067$. WT: n = 15, *Del(3.0Mb)/+*: n = 15.
Figure 9B	Two-way repeated measures ANOVA. Genotype: $F_{1,28} = 1.677$, $p = 0.2059$; Time: $F_{23,644} = 47.54$, $p < 0.0001$; Genotype × Time interaction: $F_{23,644} = 1.235$, $p = 0.2063$. WT: n = 15, *Del(3.0Mb)/+*: n = 15.
Figure 10B	1–3 day: Two-way repeated measures ANOVA. Genotype: $F_{1,28} = 0.8122$, $p = 0.3751$; Day: $F_{2,56} = 86.71$, $p < 0.0001$; Genotype × Day interaction: $F_{2,56} = 1.27$, $p = 0.2889$. Test: Two-tailed Welch's *t*-test. $t_{25.39} = 1.131$. $p = 0.2688$. WT: n = 15, *Del(3.0Mb)/+*: n = 15.
Figure 11B	Two-tailed Welch's *t*-test. $t_{23.77} = 0.0406$. $p = 0.9680$. WT: n = 15, *Del(3.0Mb)/+*: n = 15.
Figure 11C	Two-tailed Welch's *t*-test. $t_{17.76} = 0.6585$. $p = 0.5187$. WT: n = 15, *Del(3.0Mb)/+*: n = 15.
Figure 12C	Two-tailed Welch's *t*-test. Empty: $t_{27.59} = 0.3894$. $p = 0.7000$. Stranger: $t_{27.76} = 0.02859$. $p = 0.9774$. WT: n = 15, *Del(3.0Mb)/+*: n = 15.
Figure 12D	Two-tailed Welch's *t*-test. Familiar: $t_{28} = 0.3322$. $p = 0.7422$. Stranger: $t_{27.8} = 0.1378$. $p = 0.8914$. WT: n = 15, *Del(3.0Mb)/+*: n = 15.

(Table continued on next page)

(Continued)

Figure 13B	1–4 trial: Two-way repeated measures ANOVA. Genotype: $F_{1,20} = 0.2479$, $p = 0.6240$. Trial: $F_{3,60} = 48.34$, $p < 0.0001$. Genotype × Trial interaction: $F_{3,60} = 0.0582$, $p = 0.9814$. 5 trial: Two-tailed Welch's *t*-test. $t_{16.68} = 2.161$. $^{*}p = 0.0456$. WT: n = 13, *Del(3.0Mb)/+*: n = 9.
Figure 14B	Two-way repeated measures ANOVA. Genotype: $F_{1,28} = 11.07$, $^{**}p = 0.0025$. Prepulse intensity: $F_{3,84} = 83.06$, $p < 0.0001$. Genotype × Prepulse intensity interaction: $F_{3,84} = 0.5792$, $p = 0.6303$. WT: n = 15, *Del(3.0Mb)/+*: n = 15.
Figure 14C	Two-tailed Welch's *t*-test. $t_{22.96} = 2.101$. $^{*}p = 0.0468$. WT: n = 15, *Del(3.0Mb)/+*: n = 15.
Figure 15B	Two-way repeated measures ANOVA. Genotype: $F_{1,20} = 0.0569$, $p = 0.8139$. Prepulse intensity: $F_{1,20} = 0.2033$, $p = 0.6570$. Genotype × Prepulse intensity interaction: $F_{1,20} = 0.6502$, $p = 0.4295$. WT: n = 13, *Del(3.0Mb)/+*: n = 9.
Figure 16B	Two-tailed Welch's *t*-test. $t_{27.81} = 2.958$. $^{**}p = 0.0063$. WT: n = 15, *Del(3.0Mb)/+*: n = 15.
Figure 16C	Two-tailed Welch's *t*-test. $t_{27.94} = 2.27$. $^{*}p = 0.0311$. WT: n = 15, *Del(3.0Mb)/+*: n = 15.
Figure 16D	Two-tailed Welch's *t*-test. $t_{26.66} = 0.09187$. $p = 0.9275$. WT: n = 15, *Del(3.0Mb)/+*: n = 15.
Figure 17B	Two-tailed Welch's *t*-test. Familiar: $t_{27.83} = 1.545$. $p = 0.1337$ Novel: $t_{26.43} = 0.1498$. $p = 0.8820$. WT: n = 15, *Del(3.0Mb)/+*: n = 15.
Figure 17C	Two-tailed Welch's *t*-test. $t_{26.97} = 1.513$. $p = 0.1419$. WT: n = 15, *Del(3.0Mb)/+*: n = 15.

(Table continued on next page)

(Continued)

Figure 18B	Two-tailed Welch's *t*-test. Context: $t_{12.6} = 0.6943$. $p = 0.5001$. Pre-tone: $t_{15.29} = 0.1894$. $p = 0.8523$. Tone: $t_{15.19} = 2.849$. $^{*}p = 0.0117$. WT: n = 13, *Del(3.0Mb)*/+: n = 9.
Figure 19B	Two-tailed Welch's *t*-test. $t_{10.49} = 0.2675$. $p = 0.7943$. WT: n = 7, *Del(3.0Mb)*/+: n = 6.
Figure 19C	Two-tailed Welch's *t*-test. $t_{8.955} = 4.136$. $^{**}p = 0.0025$. WT: n = 7, *Del(3.0Mb)*/+: n = 6.
Figure 19D	Two-way repeated measures ANOVA. Genotype: $F_{1,11} = 8.242$, $^{*}p = 0.0152$; Session: $F_{3,33} = 20.99$, $p < 0.0001$; Genotype × Session interaction: $F_{3,33} = 2.073$, $p = 0.1228$. WT: n = 7, *Del(3.0Mb)*/+: n = 6.
Figure 19E	Two-tailed Welch's *t*-test. R early: $t_{6.376} = 0.9963$. $p = 0.3554$. R middle: $t_{10.25} = 0.3115$. $p = 0.7616$. R late: $t_{10.99} = 0.4749$. $p = 0.6442$. WT: n = 7, *Del(3.0Mb)*/+: n = 6.
Figure 19F	Two-tailed Welch's *t*-test. R early: $t_{6.302} = 0.8051$. $p = 0.4501$. R middle: $t_{10.98} = 0.3581$. $p = 0.7271$. R late: $t_{10.97} = 0.7466$. $p = 0.4710$. WT: n = 7, *Del(3.0Mb)*/+: n = 6.
Figure 20A	Two-tailed Welch's *t*-test. $t_{25.59} = 1.179$. $p = 0.2494$. WT: n = 20, *Del(3.0Mb)*/+: n = 20.
Figure 20B	Two-tailed Welch's *t*-test. $t_{37.72} = 0.7169$. $p = 0.4778$. WT: n = 20, *Del(3.0Mb)*/+: n = 20.
Figure 20C	Two-tailed Welch's *t*-test. $t_{37} = 0.3944$. $p = 0.6955$. WT: n = 19, *Del(3.0Mb)*/+: n = 20.
Figure 20D	Two-tailed Welch's *t*-test. $t_{25.64} = 0.9568$. $p = 0.3476$. WT: n = 19, *Del(3.0Mb)*/+: n = 20.

(Table continued on next page)

(Continued)

Figure 21D	Two-tailed Welch's *t*-test. N1: $t_{12.91} = 0.7473$. $p = 0.4683$. P1: $t_{11.84} = 2.869$. $^{*}p = 0.0143$. N2: $t_{12.18} = 2.876$. $^{*}p = 0.0138$. WT: n = 8, *Del(3.0Mb)/+*: n = 7.
Figure 21E	Two-tailed Welch's *t*-test. N1: $t_{6.372} = 2.342$. $p = 0.0552$. P1: $t_{7.194} = 2.140$. $p = 0.0686$. N2: $t_{12.99} = 0.9256$. $p = 0.3715$. WT: n = 8, *Del(3.0Mb)/+*: n = 7.
Figure 22A	Two-tailed Welch's *t*-test. $t_{23.48} = 1.991$. $p = 0.0583$. WT: n = 13, *Del(3.0Mb)/+*: n = 14.
Figure 22B	Two-tailed Welch's *t*-test. Phase delay: $t_{24.97} = 0.5221$. $p = 0.6062$. WT: n = 13, *Del(3.0Mb)/+*: n = 14. Phase advance: $t_{20.88} = 1.129$. $p = 0.2715$. WT: n = 13, *Del(3.0Mb)/+*: n = 13.
Figure 22C	Two-tailed Welch's *t*-test. Phase shift (left panel): $t_{15.3} = 2.616$. $^{*}p = 0.0192$. WT: n = 13, *Del(3.0Mb)/+*: n = 13. Phase shift (right panel): $t_{21.42} = 0.8958$. $p = 0.3803$. WT: n = 12, *Del(3.0Mb)/+*: n = 13.
Figure 22D	Sidak's multiple comparison after two-way repeated measure ANOVA. Genotype: $F_{1,25} = 0.3379$, $p = 0.5663$; Time: $F_{23,575} = 33.96$, $p < 0.0001$; Genotype × Time interaction: $F_{23,575} = 2.19$, $p = 0.0012$. WT vs. *Del(3.0Mb)/+*; 16 (h): $^{*}p = 0.0268$. WT: n = 14, *Del(3.0Mb)/+*: n = 13.
Figure 22E	Sidak's multiple comparison after two-way repeated measure ANOVA. Genotype: $F_{1,25} = 0.2003$, $p = 0.6583$; Time: $F_{23,575} = 82.19$, $p < 0.0001$; Genotype × Time interaction: $F_{23,575} = 1.86$, $p = 0.0090$. WT vs. *Del(3.0Mb)/+*; 22 (h): $^{*}p = 0.0337$, 0 (h): $^{*}p = 0.0411$. WT: n = 14, *Del(3.0Mb)/+*: n = 13.

Table 5. The efficiency of generating *Del(3.0Mb)/+* mice.

Deletion model	Embryos injected[a]	Transferred[b] (%: b/a)	Pups born[c] (%: c/b)	Weaning[d] (%: d/c)	Desired mutants[e] (%: e/d)
Del(3.0Mb)/+	1119	644 (57.6%)	95 (14.8%)	74 (77.9%)	4 (5.4%)

Table 6. Neonatal mortality rate of *Del(3.0Mb)/+* mice before weaning.

Number of pups		Number of deaths		Number of weaning	
WT[a]	*Del(3.0Mb)/+*[b]	WT[c] (%: c/a)	*Del(3.0Mb)/+*[d] (%: d/b)	WT[e] (%: e/a)	*Del(3.0Mb)/+*[f] (%: f/b)
265	211	77 (29.1%)	149 (70.6%)	188 (70.9%)	62 (29.4%)

Table 7. Appearance rate of cardiovascular and thymic abnormalities observed in *Del(3.0Mb)/+* embryos (E18.5).

Genotype	Number of embryos	Phenotype		
		IAA	ARSA	Thymus
WT	18	0 (0%)	0 (0%)	0 (0%)
Del(3.0Mb)/+	15	2 (13.3%)	1 (6.7%)	7 (46.7%)

IAA, interrupted aortic arch; ARSA, aberrant right subclavian artery; Thymus, thymic hypoplasia.

Table 8. Number of potential off-target sites for sgRNAs.

sgRNA	sgRNA target sequences	Number of off-target	
		20 mer + PAM	12 mer + PAM
Pi4ka sg1	CAGGACTGGGACTCGAGACGGGG	0	0
Pi4ka sg2	ATGCGGCCCCACAGATCTGGAGG	0	14
Hira sg1	GAGGAGGTCGCCTATTGTCCAGG	0	0
Hira sg2	GGTAGAAGGAGTGGGCTAACAGG	0	4

Underlined parts indicate PAM sequences.

Table 9. Locations of potential off-target sites of Pi4ka sg2 and Hira sg2.

sgRNA	Enter position	Sequences (12 mer + PAM)	Location
Pi4ka sg2	chr3:49721756-49721770	**CC**T**CC**AGATCTGTGG	Intergenic region
	chr3:83575053-83575067	**CC**T**CC**AGATCTGTGG	Intergenic region
	chr3:88206235-88206249	**CC**T**CC**AGATCTGTGG	Intergenic region
	chr5:140791666-140791680	**CC**T**CC**AGATCTGTGG	*Gna12* (Guanine nucleotide binding protein, alpha 12) intron1
	chr5:151302307-151302321	**CC**T**CC**AGATCTGTGG	*Gm42906* intron1
	chr11:35452553-35452567	**CC**C**CC**AGATCTGTGG	*Slit3* (Slit guidance ligand3) intron4
	chr16:73461333-73461347	**CC**T**CC**AGATCTGTGG	Intergenic region
	chr1:159751367-159751381	CCACAGATCTGG**GGG**	*Tnr* (Tenascin R) intron2
	chr4:64139676-64139690	CCACAGATCTGG**GGG**	*8030451A03Rik* intron4
	chr8:26248064-26248078	CCACAGATCTGG**GGG**	Intergenic region
	chr10:32927063-32927077	CCACAGATCTGG**AGG**	*Gm47823* intron1
	chr13:32065409-32065423	CCACAGATCTGG**GGG**	*Gmds* (GDP-mannose 4, 6-dehydratase) intron7
	chr14:67643862-67643876	CCACAGATCTGG**AGG**	Intergenic region
	chr18:12229915-12229929	CCACAGATCTGG**AGG**	*Npc1* (NPC intracellular cholesterol transpoter1) intron1
Hira sg2	chr2:26605340-26605354	**CC**G**CC**GTTAGCCCACTC	*Gm20532* intron3
	chr4:133475054-133475068	GAGTGGGCTAAC**AGG**	Intergenic region
	chr12:108133647-108133661	GAGTGGGCTAAC**AGG**	*Setd3* (SET domain containing 3) intron6
	chr15:81544993-81545007	GAGTGGGCTAAC**TGG**	Intergenic region

Mismatch bases are indicated in red.

PAM sequences (NGG or CCN) are indicated in bold.